UCRL-ID--104890
DE91 001084

Penetration of Yawed Projectiles

John E. Reaugh

Abstract

We used computer simulations and experiments to study the penetration of tungsten-alloy projectiles into a thick, armored steel target. These projectiles, with length-to-diameter ratios of 4, strike the target with severe yaws, up to 90° (side-on impact), such as might be induced in an originally longer projectile by a multiple-spaced plate array. In this study, we focus on the terminal ballistics of these projectiles and ignore how the yaw was induced. We found that the minimum penetration depth occurs at 90° yaw. This case is well approximated by the two-dimensional plane-strain penetration of a side-on cylinder. The ratio of penetration depth to diameter, *P:D*, for this case is larger than that for a sphere because the plane-strain geometry lacks hoop stress, which is activated in axisymmetric geometry. A more surprising result of our work is that the penetration at 60° yaw is only slightly deeper than that of the side-on impact.

Introduction

We used JOY, a three-dimensional Eulerian computer simulation program developed at Lawrence Livermore National Laboratory (LLNL),[1] to study the penetration mechanics of severely yawed projectiles. In previous studies,[2,3] we used the two-dimensional program GLO, under development at LLNL, to study the penetration of eroding tungsten rods into steel targets at normal incidence. We showed that for rods with length-to-diameter ratio $L:D = 10$, the computer simulations of penetration depth and crater diameter were insensitive to the value of the projectile strength and considerably more sensitive to the value of target strength.

The target steel in the experiments was AISI 4340 steel, in bricks $6 \times 6 \times 2.5$ in. thick, heat-treated to a Rockwell hardness of R_c 35. We also cut tensile specimens from 4340 steel hardened to R_c 35 and performed standard engineering tensile tests. We augmented the standard measurement by continually monitoring the diameter profile through the neck region. Using the procedure of Norris et al.[4] and HEMP simulations of the tensile test,[5] we fitted a flow stress curve to the load-elongation and load-neck-area data through maximum load up to fracture. In these simulations, we used only the initial yield stress from that fit, 10.3 kbar. From previous studies, we determined that the use of both work-hardening (as determined from the engineering tensile tests) and thermal-softening (following the model described by Steinberg et al.[6]) resulted in approximately the same computed penetration depth as the use of a constant flow stress. We used a nominal strength of 17 kbar to describe the tungsten sinter alloy W2. Table 1 lists the material properties for steel and tungsten that we used in these simulations.

In previous studies with GLO, we determined that 5 to 10 square zones in the projectile radius throughout the crater area were adequate to define the penetration depth and crater diameter. With GLO, we have routinely used 10 zones in the projectile radius to provide somewhat better resolution of the projectile residue and have noticed improvements with up to 20 zones in the radius for projectiles with $L:D \leq 1$. With three-dimensional programs, however, we must exercise restraint on the resolution specified because it is relatively easy to define a calculational mesh that does not fit the computer at hand.[7]

We performed a computer simulation of the normal impact of an $L:D = 4$ tungsten alloy W2 projectile into the 4340 steel target at 1.75 km/s. With 1.2-mm cubical zones (about 2-1/2 zones in the projectile radius of 3.175 mm), the penetration depth from JOY (three dimensional with two symmetry planes) was similar to that from a GLO (two dimensional axisymmetric)

Table 1. Material properties used in the computer simulations.

Property	W2 tungsten	Steel
Density, ρ_0 (g/cm^3)	18.5	7.83
Bulk modulus, K (Mbar)	3.12	1.59
C_1 (Mbar)[a]	2.2	1.6
Shear modulus, G (Mbar)	1.6	0.77
Yield stress, Y (kbar)	17	10.3
Gruneissen ratio,[a] Γ	1.54	1.36

[a] The equation of state for pressure P in Mbar is given by:

$$P = K\mu + C_1\mu^2 + \Gamma e\rho ,$$

where e is energy density in 10^{12} erg/g (Mbar · cm^3/g), ρ is density in g/cm^3, and μ is excess compression, $\mu = \rho/\rho_0 - 1$.

simulation with 0.3-mm-square zones, but the crater diameter was inadequately defined. When we used 0.6-mm-square zones transverse to the projectile axis, keeping 1.2-mm zones in the axial direction, we maintained a crater depth and diameter comparable to the axisymmetric simulation.

For all of the results reported here, we kept the zone size in the directions transverse to the flight axis at 0.6 mm and decreased the zone size along the flight axis with increasing obliquity, using 0.6-mm cubes for the 90° yaw case. This maintained the problem size at about 400,000 zones for intermediate yaws with a single plane of symmetry.

Results of the experiments

We fired $L{:}D = 4$ tungsten alloy rods into 4340 R_c 35 steel on another program.[8] Table 2 lists the measured penetration depths for the nominal velocity of 1.75 km/s. In Fig. 1, we compare the crater profile taken from a pencil rubbing of the sectioned crater with the GLO and JOY simulations.

Results of the simulations

We present the results of the simulations in Figs. 2–13, which view the projectile and target cut at the plane of symmetry for yaw angles of 0 (normal impact, Figs. 2–4), 30 (Figs. 5–7), 60 (Figs. 8–10), and 90° (side-on impact, Figs. 11–13). In the appendix, we show the projectile and steel target boundaries in the plane of symmetry for a more quantitative evolution of the cratering process. A comparison of Fig. 4 with Figs. 7, 10, and 13 qualitatively

Table 2. Penetration of a 25.4-mm-long, $L:D = 4$ tungsten alloy W2 projectile into 4340 steel.

Projectile velocity (km/s)	Target hardness	Penetration depth (cm)
1.73	R_C 35	3.48
1.76	R_C 34	3.60

shows that the transverse crater width is significantly larger for the yawed projectiles than it is for the normal impact.

Indeed, after considering the 90° yaw case (side-on impact), we find that for a long enough rod, the crater profile must approach that of the two-dimensional plane-strain penetration of a cylinder. We performed this simulation in GLO and present the results by an overlay of the crater profiles in Fig. 14. As the $L:D$ ratio of the yawed projectile approaches 1, the penetration per unit diameter will approach that of a sphere. If we reduce the projectile $L:D$ still further, the penetration per unit diameter at 90° yaw (penny striking edgewise) will approach the penetration per unit length of a "long-rod" projectile in plane strain.

A summary of the penetration depth from the simulations is given in Table 3 and Fig. 15 as a function of yaw angle. Perhaps the least expected of these results is that for the $L:D = 4$ projectile, a yaw angle of 60° (and presumably even somewhat less) results in little more penetration depth than the side-on result.

Table 3. Computed penetration depth of yawed tungsten projectiles (25.4 mm long, $L:D = 4$) into steel at 1.75 km/s.

Yaw angle (deg)	Penetration depth (cm)
0	3.60
30	2.42
60	1.45
90	1.40

Summary

We have performed three-dimensional computer simulations of an $L{:}D = 4$ projectile into armor steel at yaw angles of 0 (normal impact), 30, 60, and 90° (side-on impact). Where experimental data are available, the simulations are in quantitative agreement for crater depth and shape. Perhaps the most surprising of our results is that the penetration depths for 60 and 90° yaw are similar. The implication is important for designing spaced armor. At a constant rotation rate, the time needed (and hence the space needed) to rotate 60° is only two-thirds of that required for 90°.

Acknowledgments

The author thanks Estella McGuire for performing the computer simulations using the HEMP, GLO, and JOY computer programs, and Bruce Cunningham for providing the experimental results at normal incidence.

This work was sponsored by the Defense Advanced Research Projects Agency.

References

1. R. Couch, E. Albright, and N. Alexander, *The JOY Computer Code,* Lawrence Livermore National Laboratory, Livermore, CA, UCID-19688 (1983).

2. M. L. Wilkins and J. E. Reaugh, *Computer Simulations of Ballistic Experiments,* Lawrence Livermore National Laboratory, Livermore, CA, UCRL-95774 (1987).

3. A. C. Holt, J. E. Reaugh, and B. J. Cunningham, *A Study of the Influence of Projectile Shape on Penetration of a Metal Half-Space,* Lawrence Livermore National Laboratory, Livermore, CA, UCRL-98735 (1989).

4. D. N. Norris, Jr., B. Moran, J. K. Scudder, and D. F. Quinones, "A Computer Simulation of the Tensile Test," *J. Mech. Phys. Solids* **26**, 1–19 (1978).

5. M. L. Wilkins, "Calculation of Elastic-Plastic Flow," in *Methods of Computational Physics,* vol. 3, B. Alder, S. Fernback, and M. Rotenberg, Eds. (Academic Press, New York, 1964), pp. 211–263.

6. D. J. Steinberg, S. G. Cochran, and M. W. Guinan, "A Constitutive Model for Metals Applicable at High-Strain Rate," *J. Appl. Phys.* **51**, 1498–1504 (1980).

7. These simulations were performed on a CRAY Y/MP 8/32 computer and required approximately 8 million words of memory for the 400,000 zone calculations.

8. B. J. Cunningham, Lawrence Livermore National Laboratory, Livermore, CA, private communication (1989).

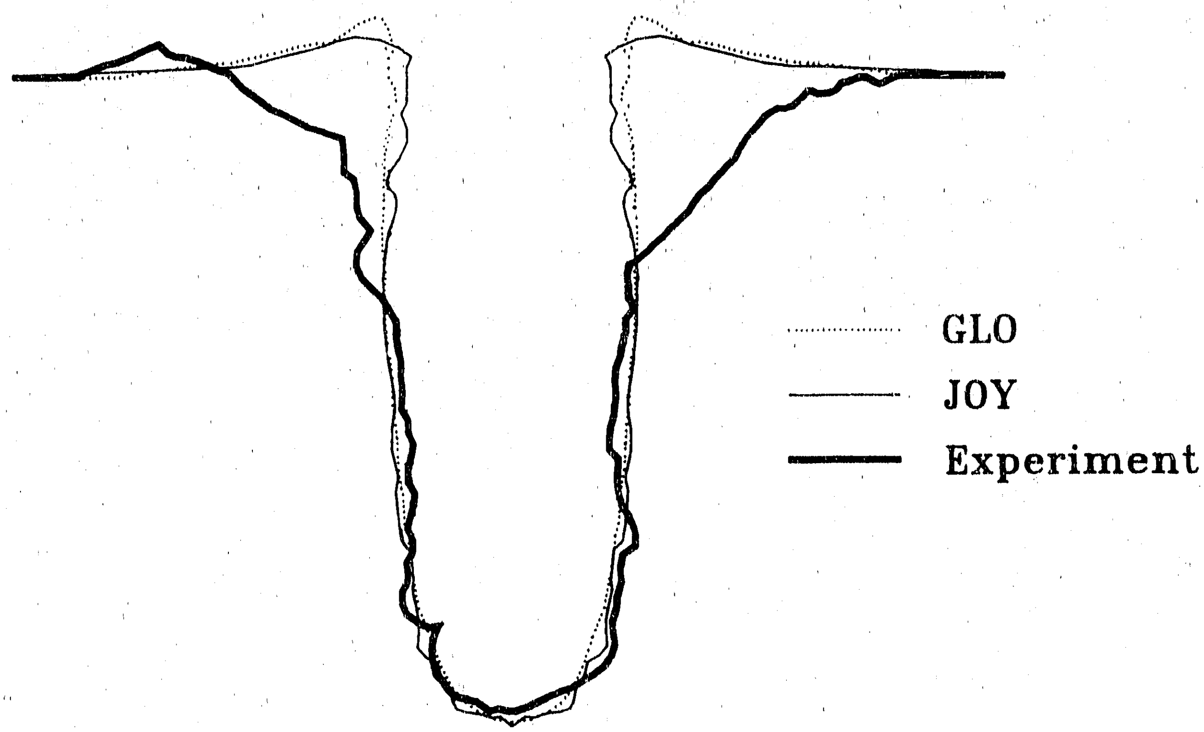

Figure 1. Crater profile from GLO (dotted line) and JOY simulation (narrow solid line) compared with the cross-sectioned experimental crater (heavy solid line). Projectile is 25.4-mm-long, $L:D = 4$ tungsten alloy at 1.75 km/s into steel.

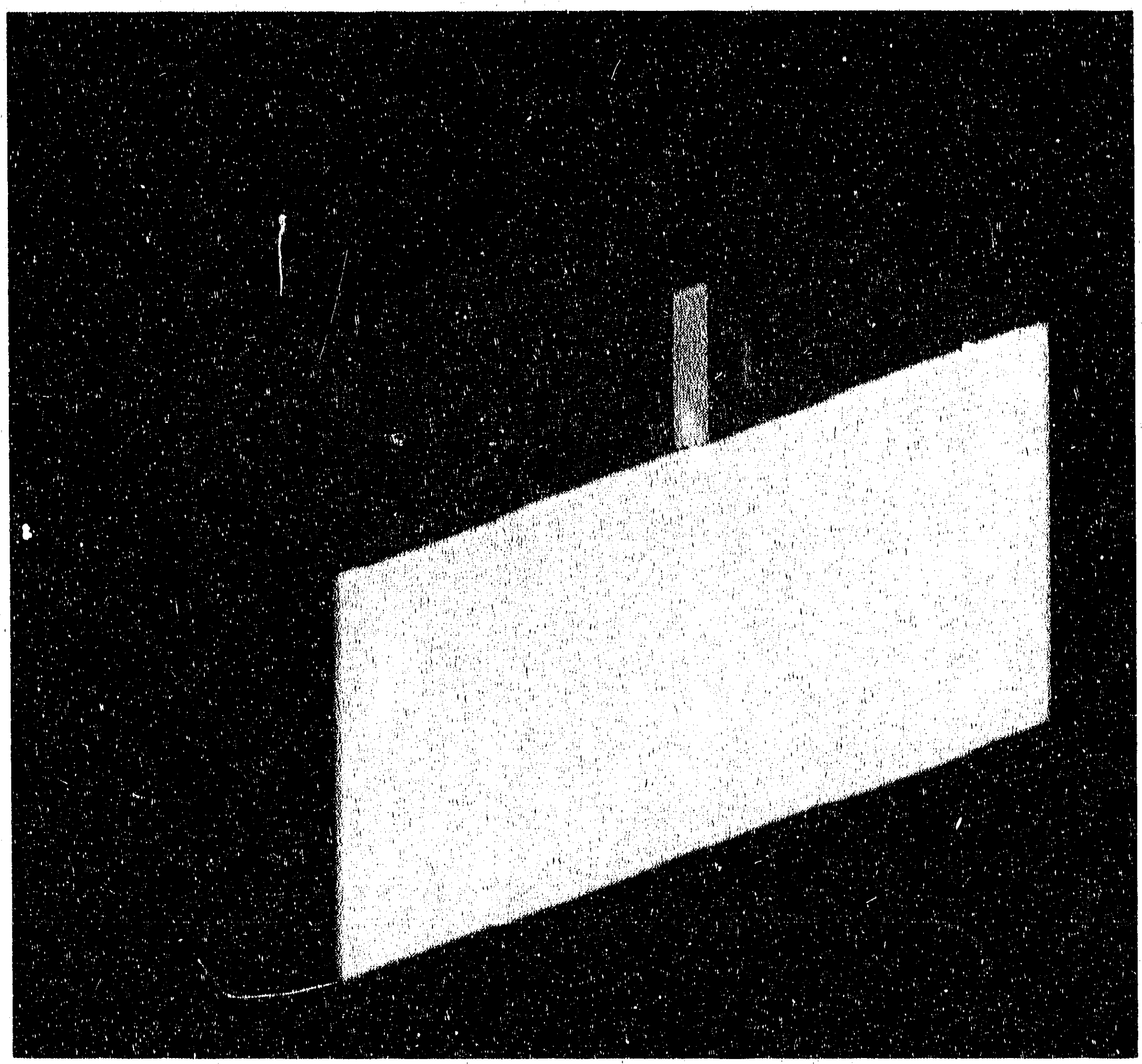

Figure 2. Computer simulation of a 25.4-mm-long, $L{:}D = 4$ tungsten alloy projectile at 0° yaw into steel at 1.75 km/s. Time = 0.

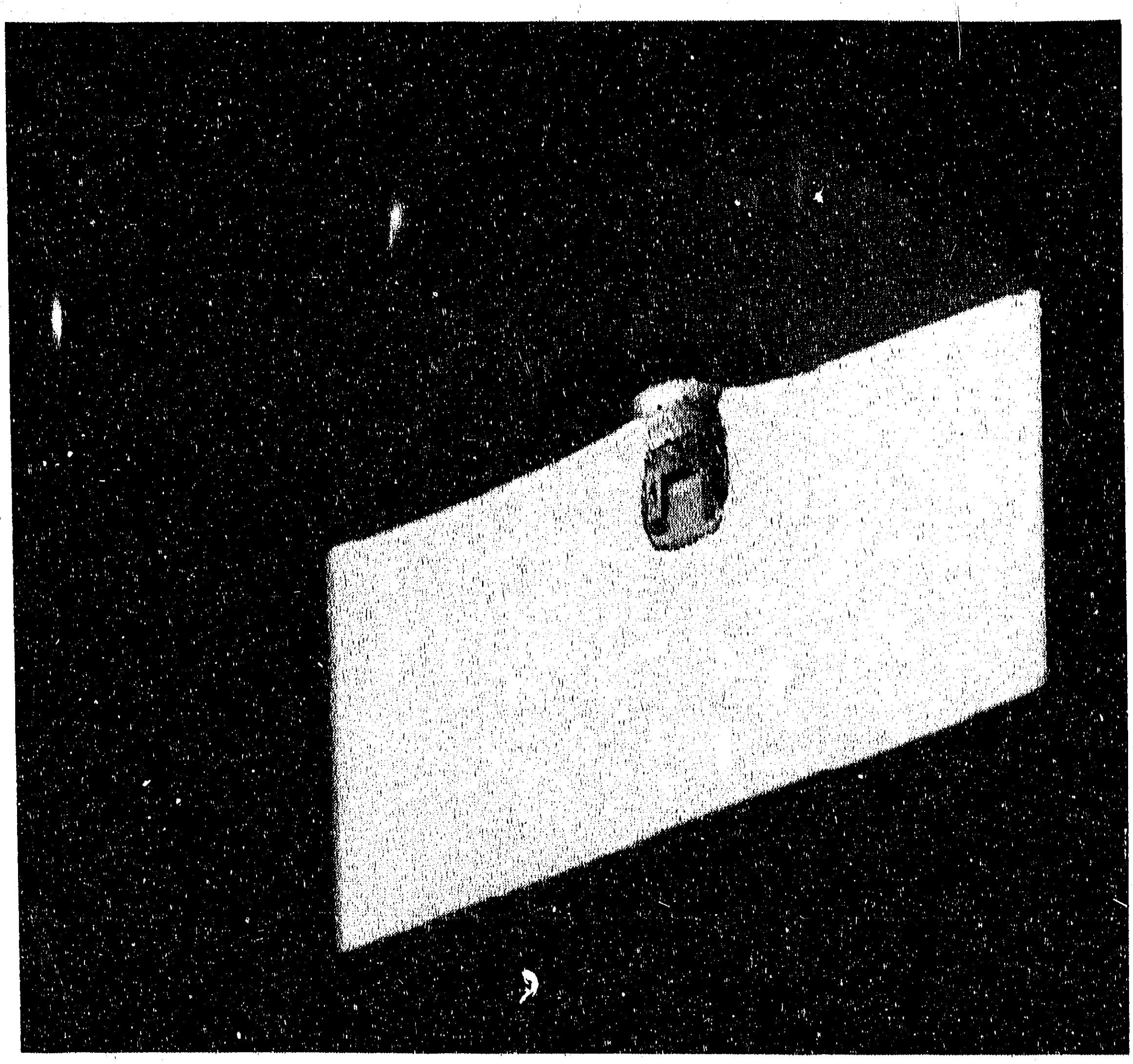

Figure 3. Computer simulation of a 25.4-mm-long, $L{:}D = 4$ tungsten alloy projectile at 0° yaw into steel at 1.75 km/s. Time = 20 μs.

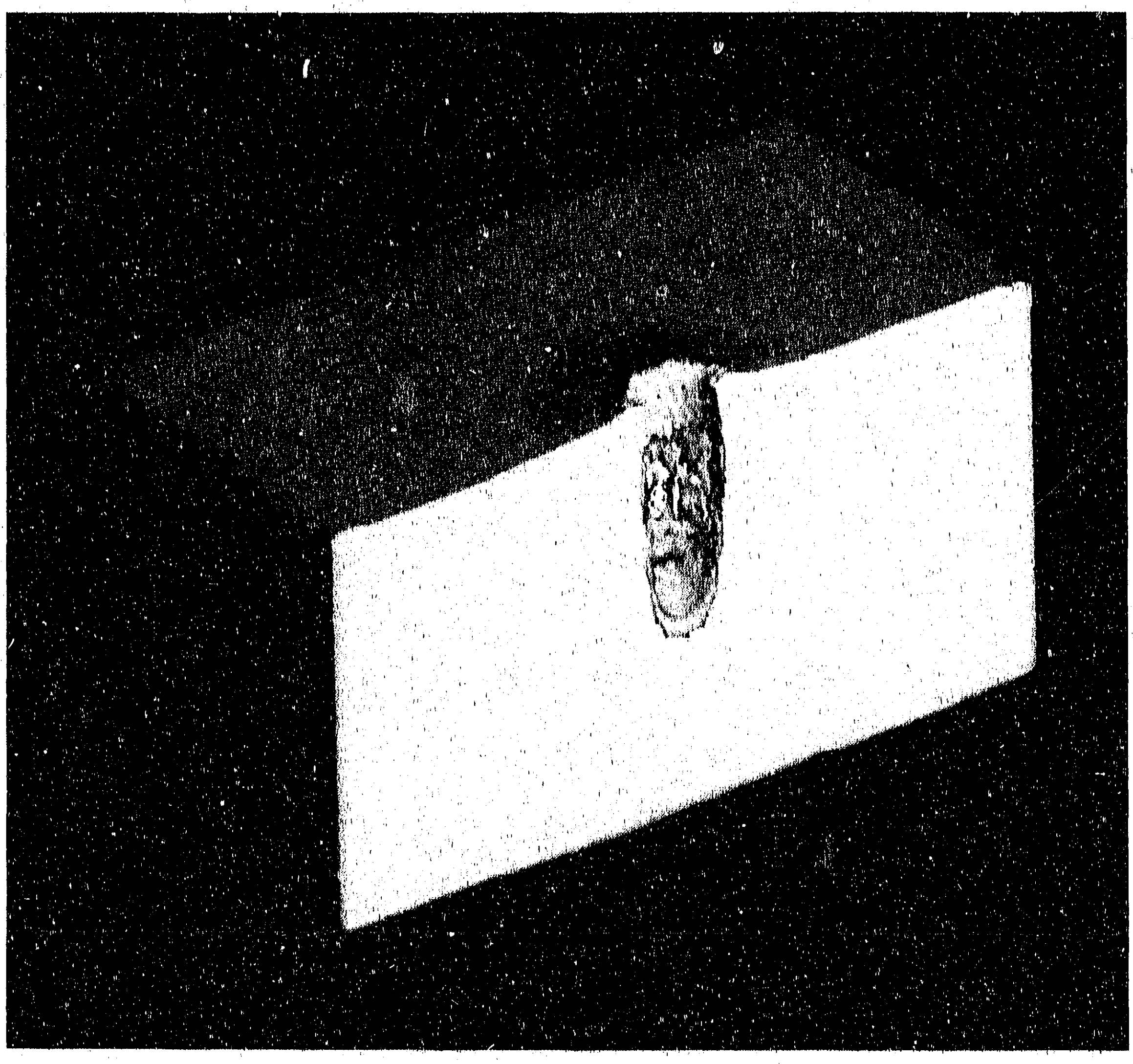

Figure 4. Computer simulation of a 25.4-mm-long, $L{:}D = 4$ tungsten alloy projectile at 0° yaw into steel at 1.75 km/s. Time = 50 μs.

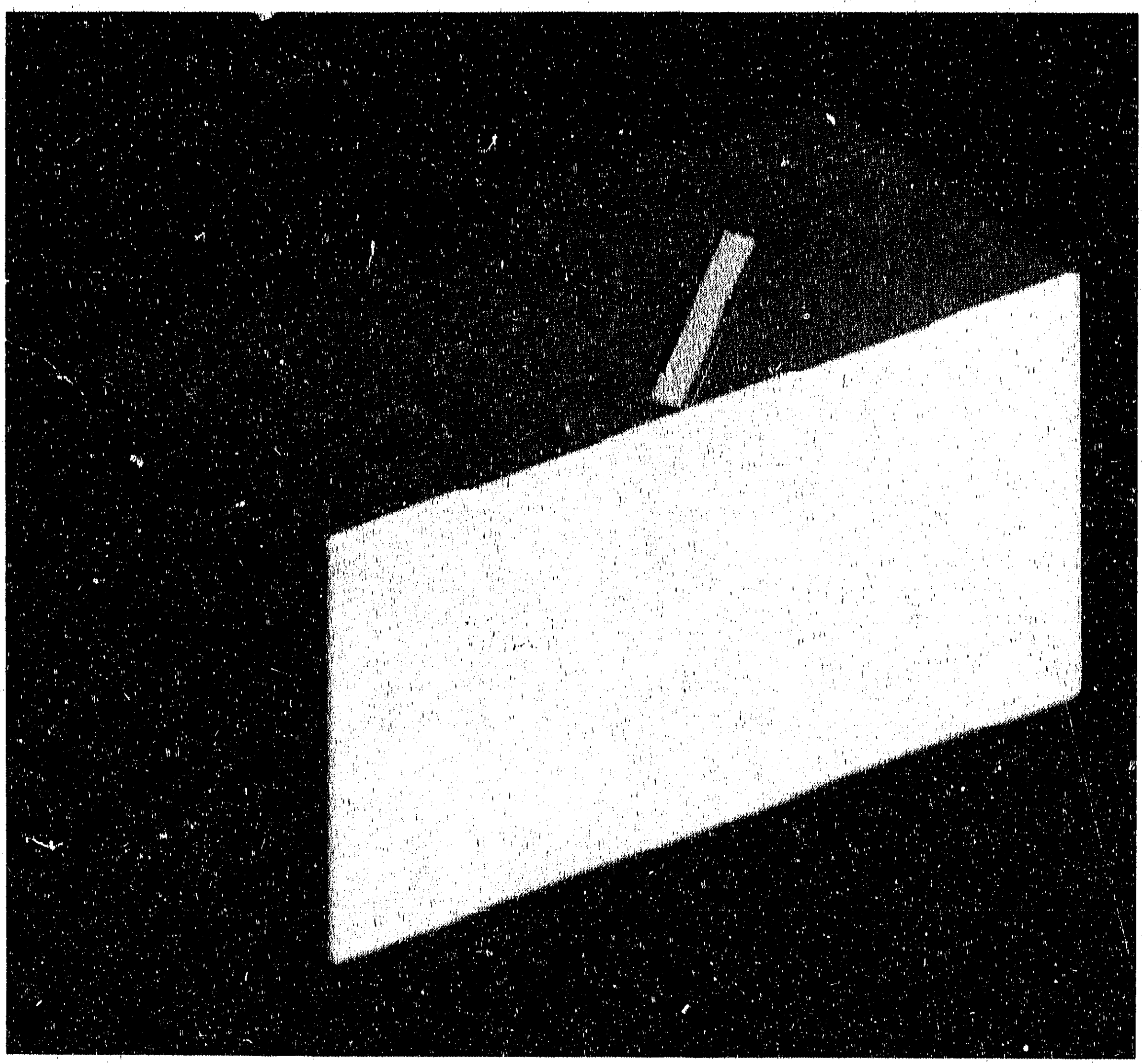

Figure 5. Computer simulation of a 25.4-mm-long, $L{:}D = 4$ tungsten alloy projectile at 30° yaw into steel at 1.75 km/s. Time = 0.

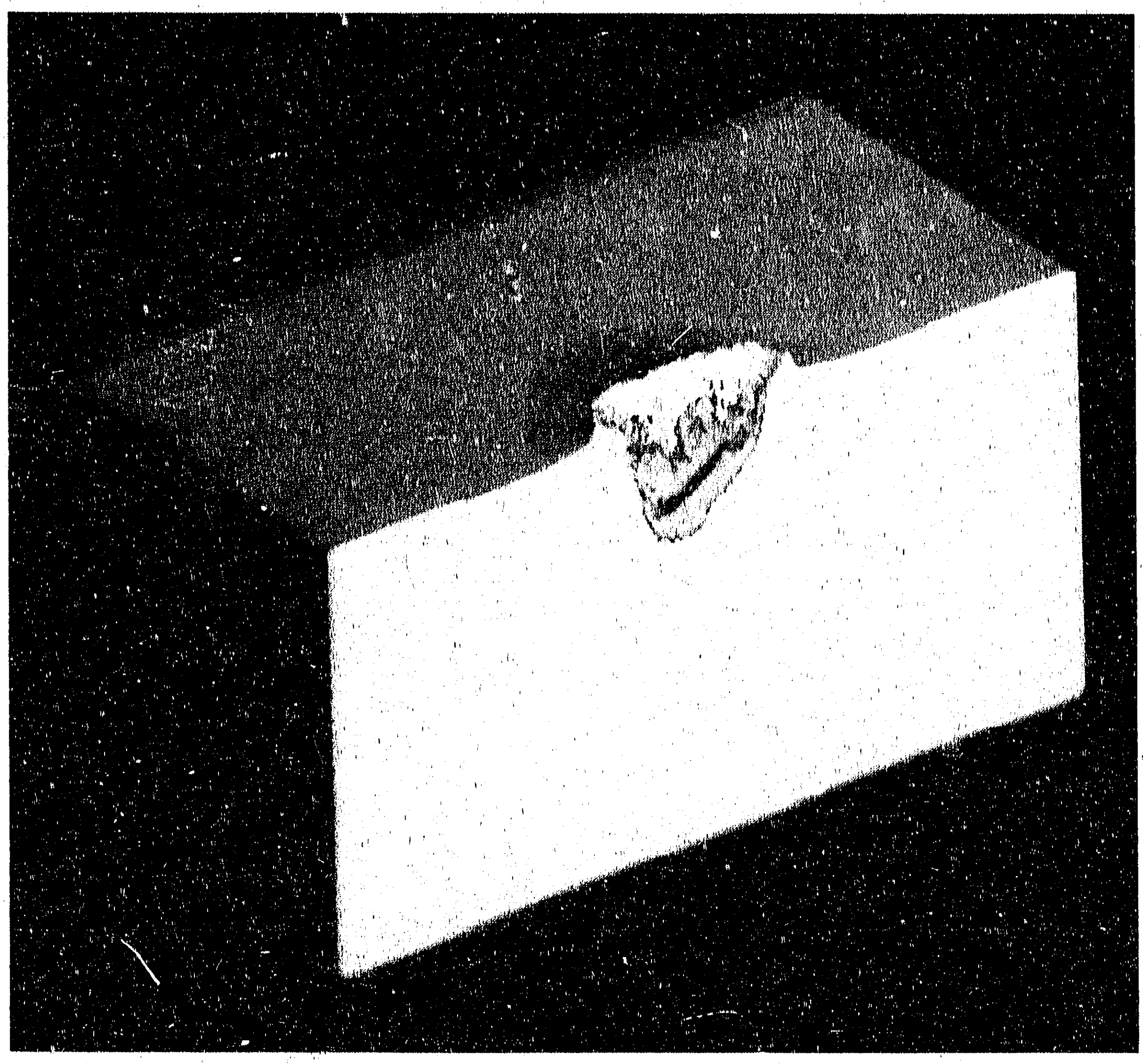

Figure 6. Computer simulation of a 25.4-mm-long, $L{:}D = 4$ tungsten alloy projectile at 30° yaw into steel at 1.75 km/s. Time = 20 μs.

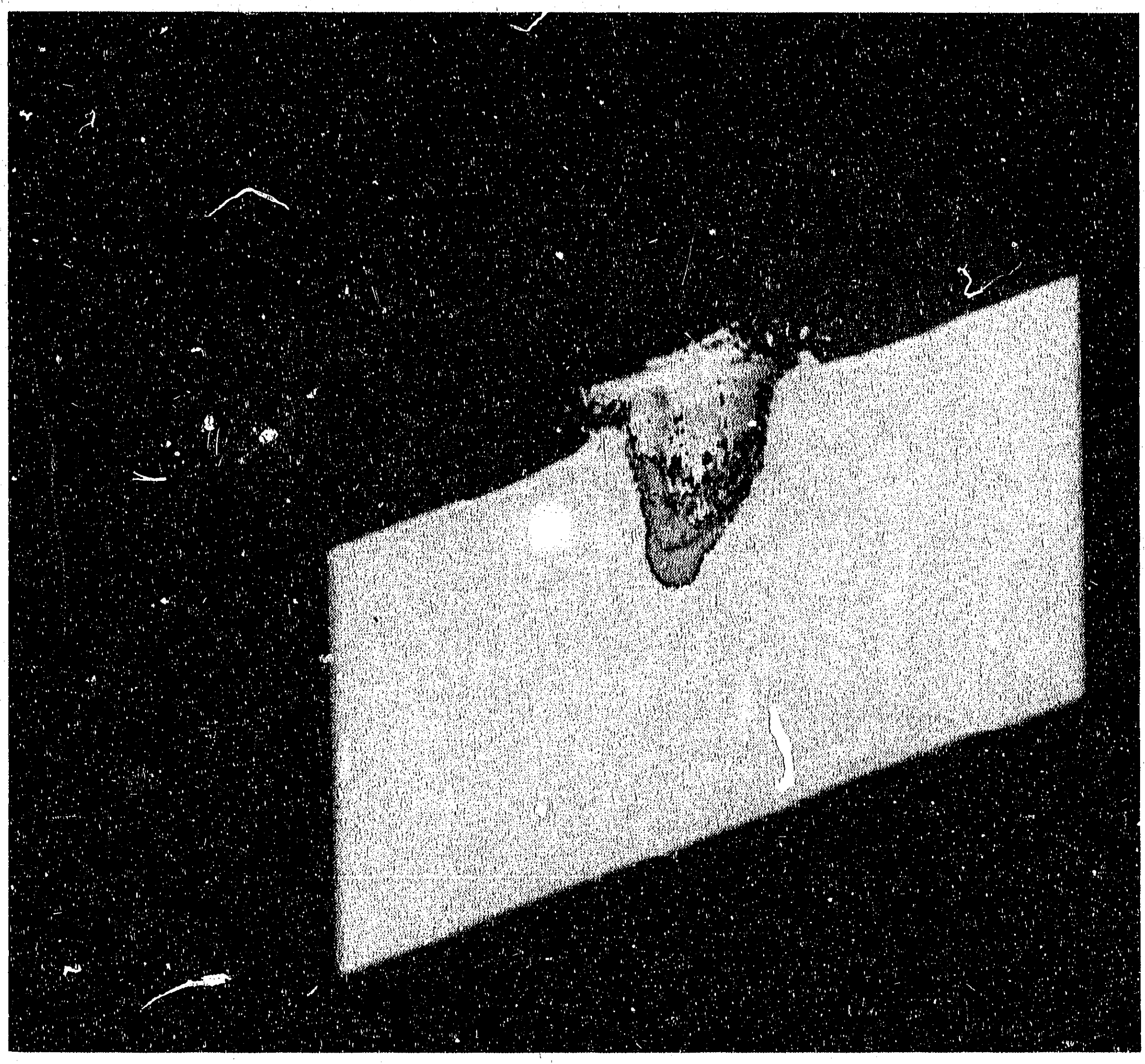

Figure 7. Computer simulation of a 25.4-mm-long, $L{:}D = 4$ tungsten alloy projectile at 30° yaw into steel at 1.75 km/s. Time = 45 μs.

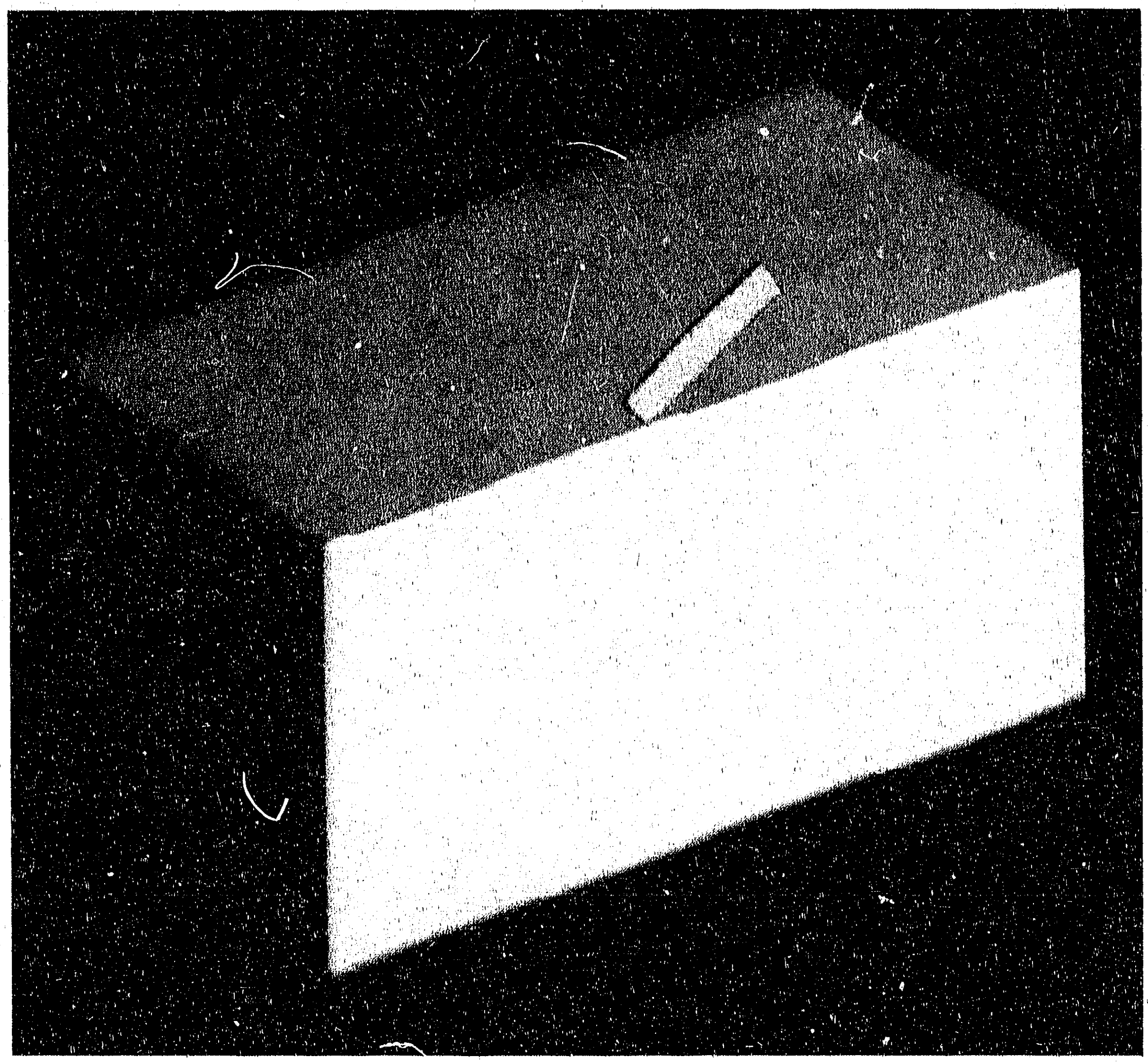

Figure 8. Computer simulation of a 25.4-mm-long, *L:D* = 4 tungsten alloy projectile at 60° yaw into steel at 1.75 km/s. Time = 0.

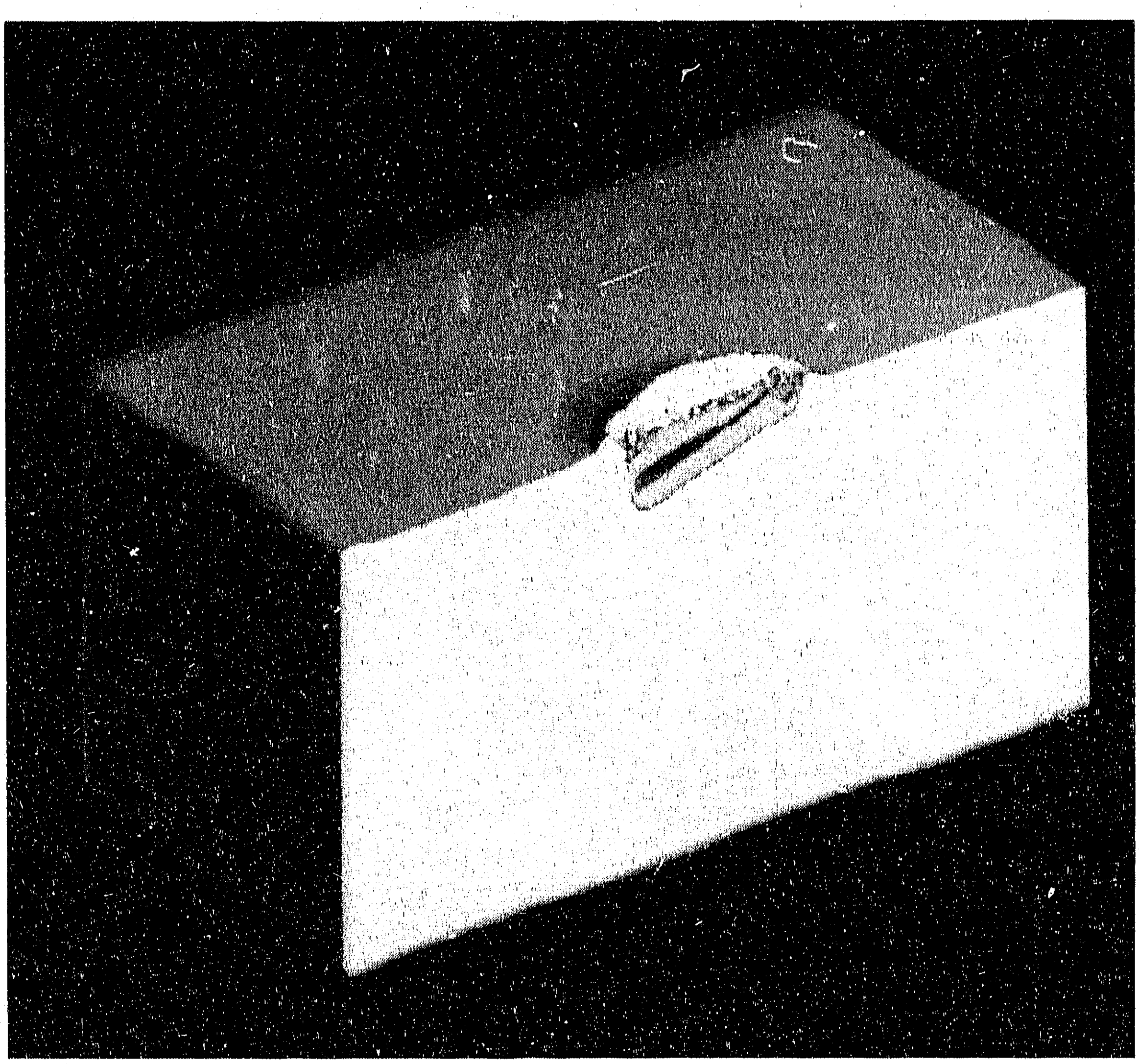

Figure 9. Computer simulation of a 25.4-mm-long, *L*:*D* = 4 tungsten alloy projectile at 60° yaw into steel at 1.75 km/s. Time = 10 μs.

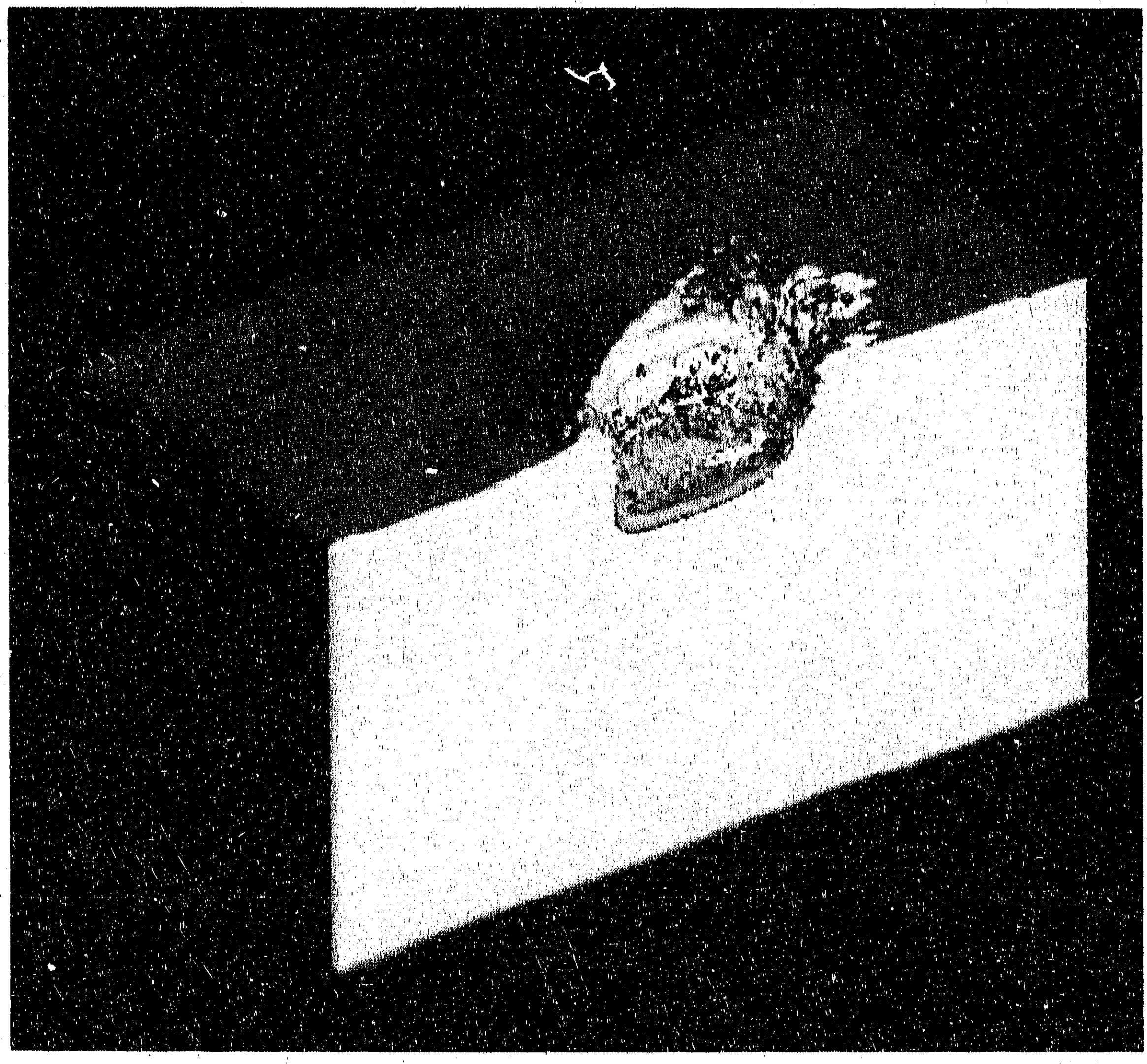

Figure 10. Computer simulation of a 25.4-mm-long, *L:D* = 4 tungsten alloy projectile at 60° yaw into steel at 1.75 km/s. Time = 45 μs.

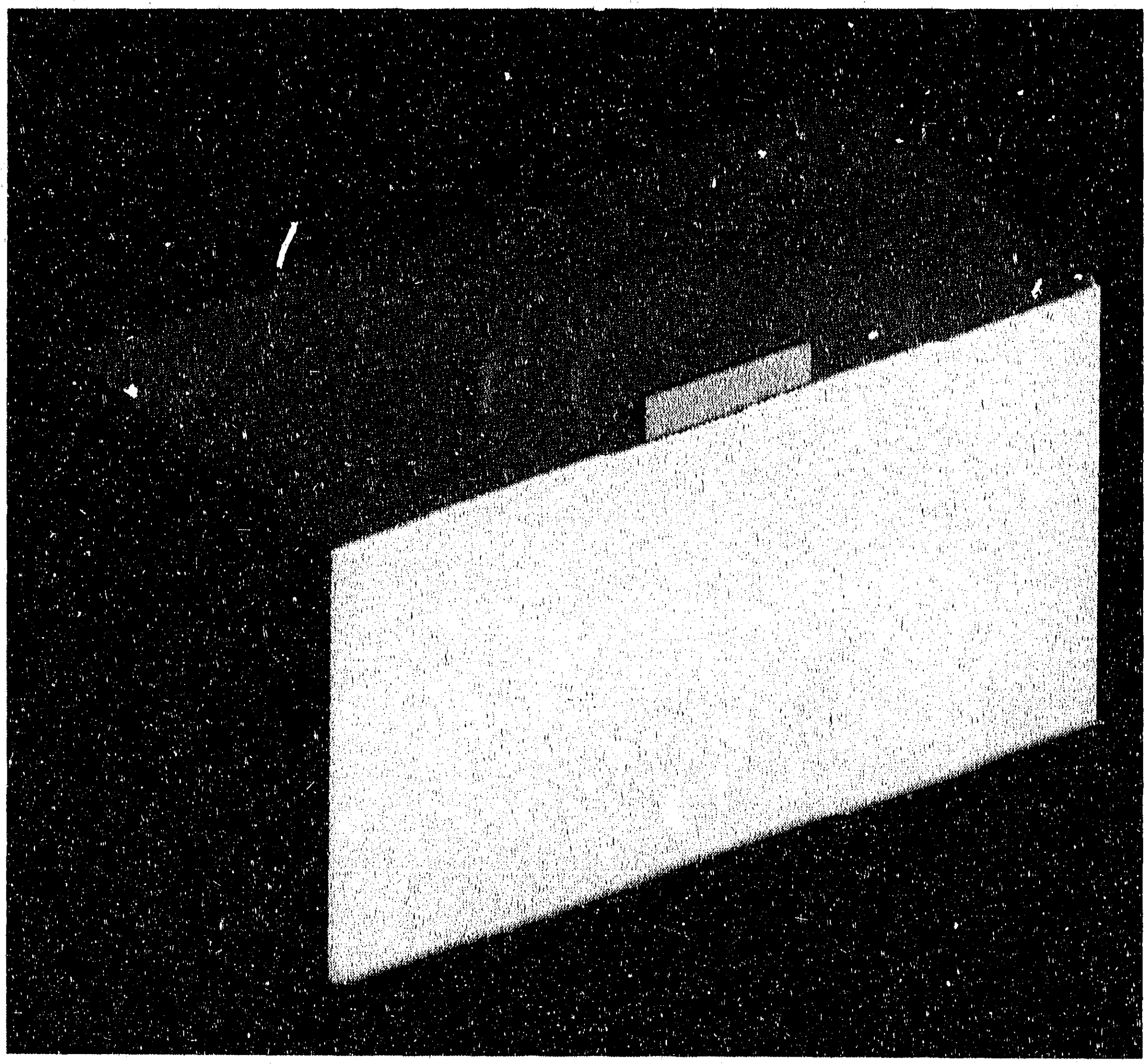

Figure 11. Computer simulation of a 25.4-mm-long, $L:D = 4$ tungsten alloy projectile at 90° yaw into steel at 1.75 km/s. Time = 0.

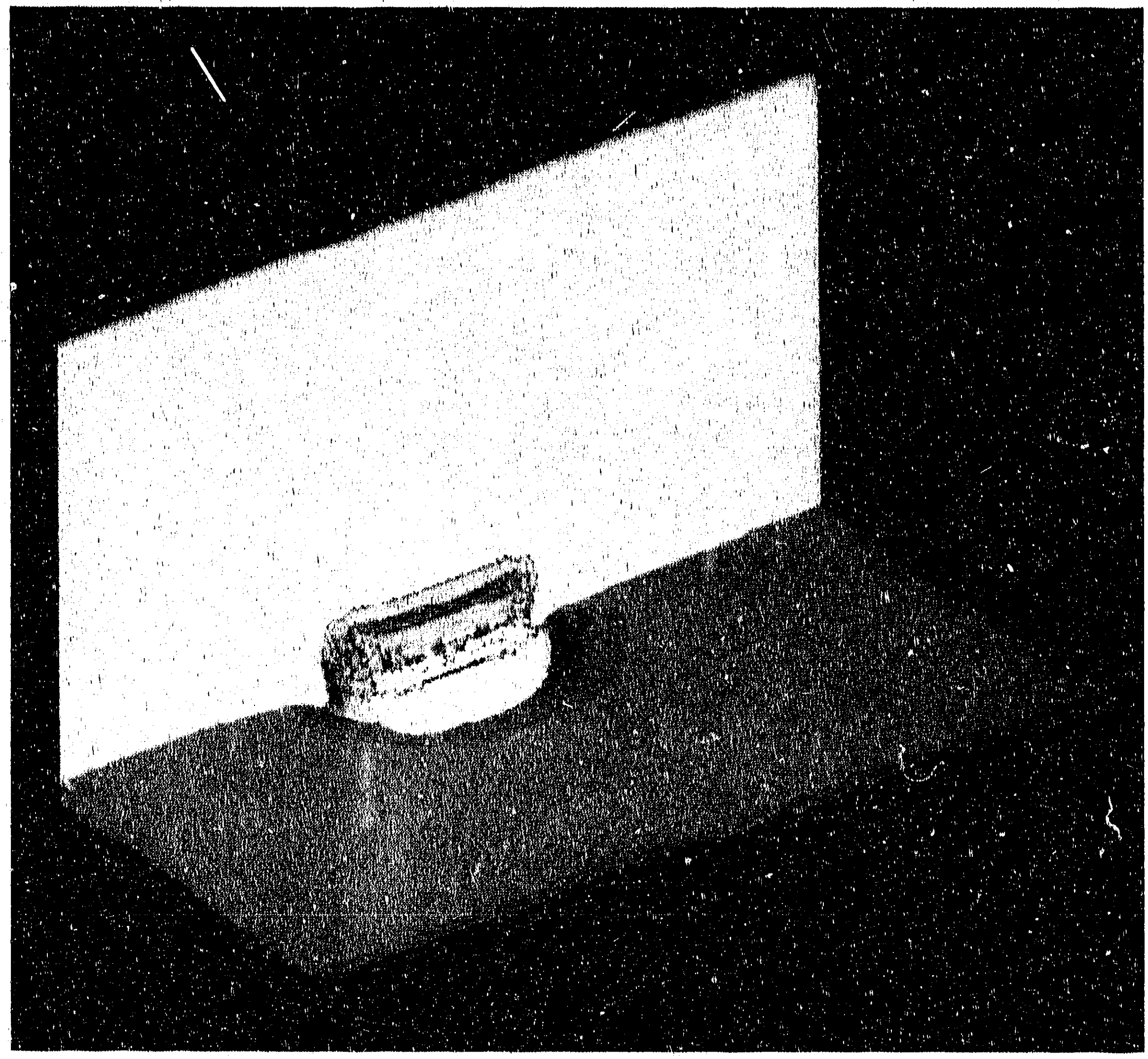

Figure 12. Computer simulation of a 25.4-mm-long, $L{:}D = 4$ tungsten alloy projectile at 90° yaw into steel at 1.75 km/s. Time = 10 μs.

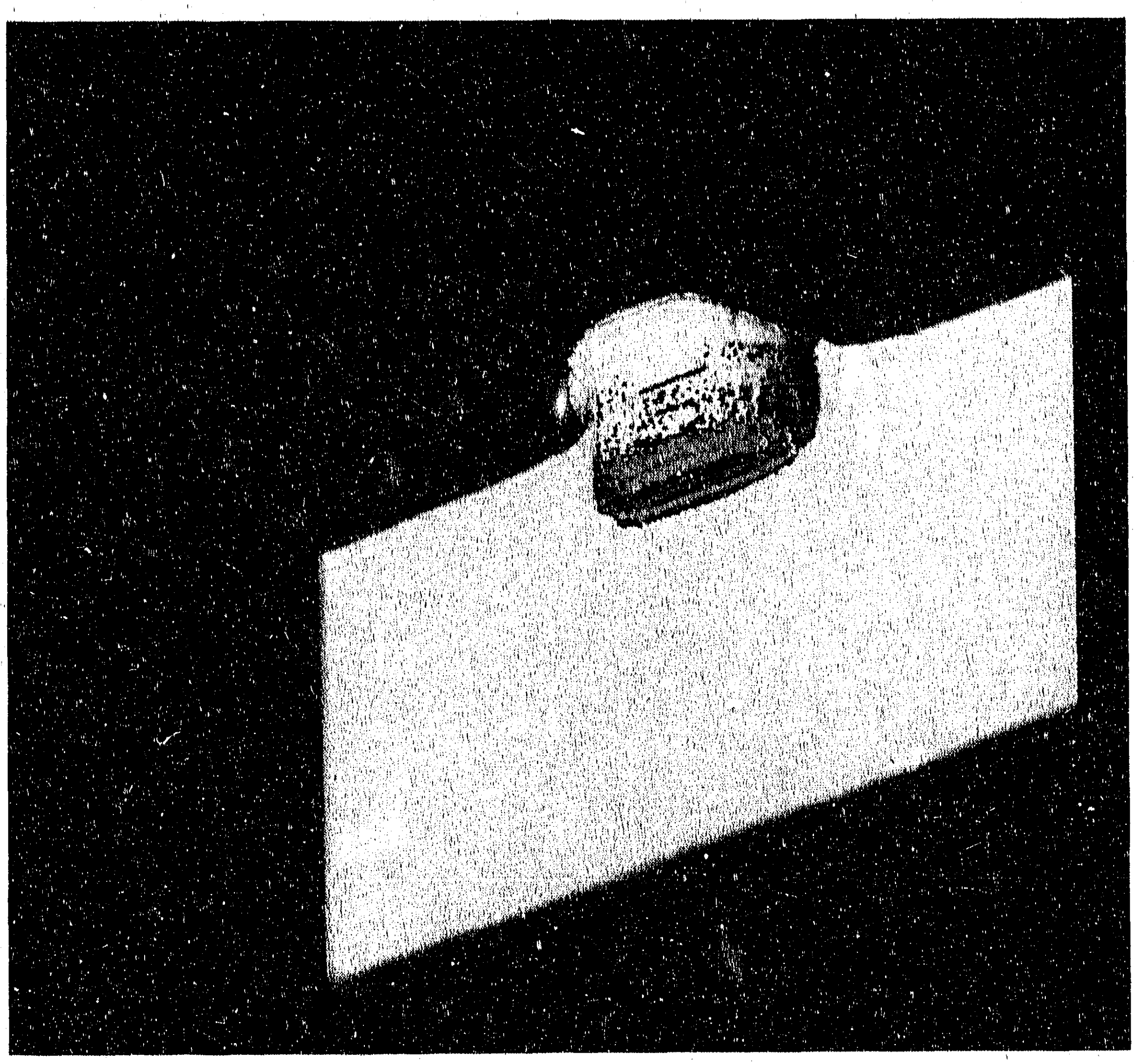

Figure 13. Computer simulation of a 25.4-mm-long, $L:D = 4$ tungsten alloy projectile at 90° yaw into steel at 1.75 km/s. Time = 25 μs.

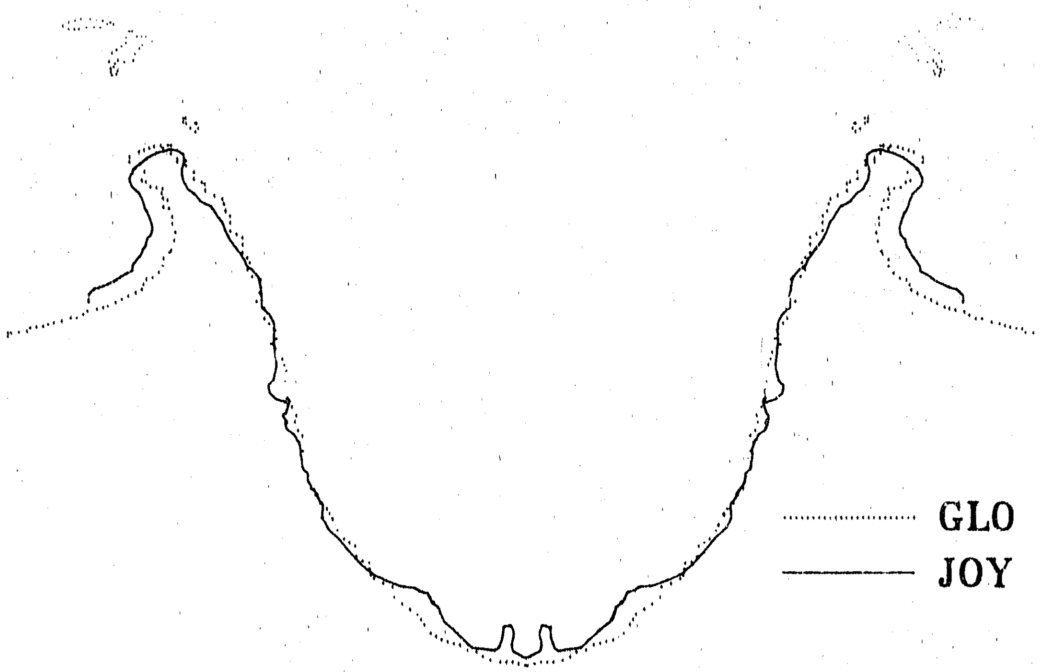

Figure 14. Comparison of transverse crater profiles from GLO (plane strain, dotted line) and JOY (90° yaw, solid line).

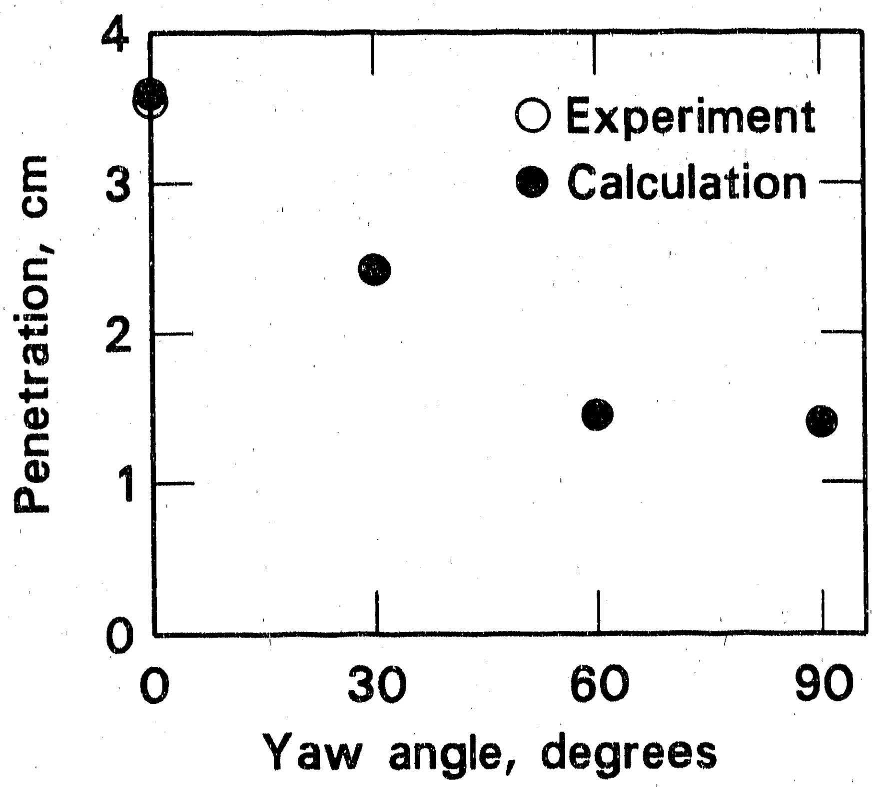

Figure 15. Penetration depth of a yawed tungsten alloy projectile into armor steel at 1.75 km/s. Projectile length is 25.4 mm, and diameter is 6.35 mm.

Appendix A

We present here the computed material boundaries in the plane of symmetry for the four three-dimensional computer simulations. The projectile is a 25.4-mm-long, $L:D = 4$ tungsten alloy at 1.75 km/s fired into a steel target at various yaw angles.

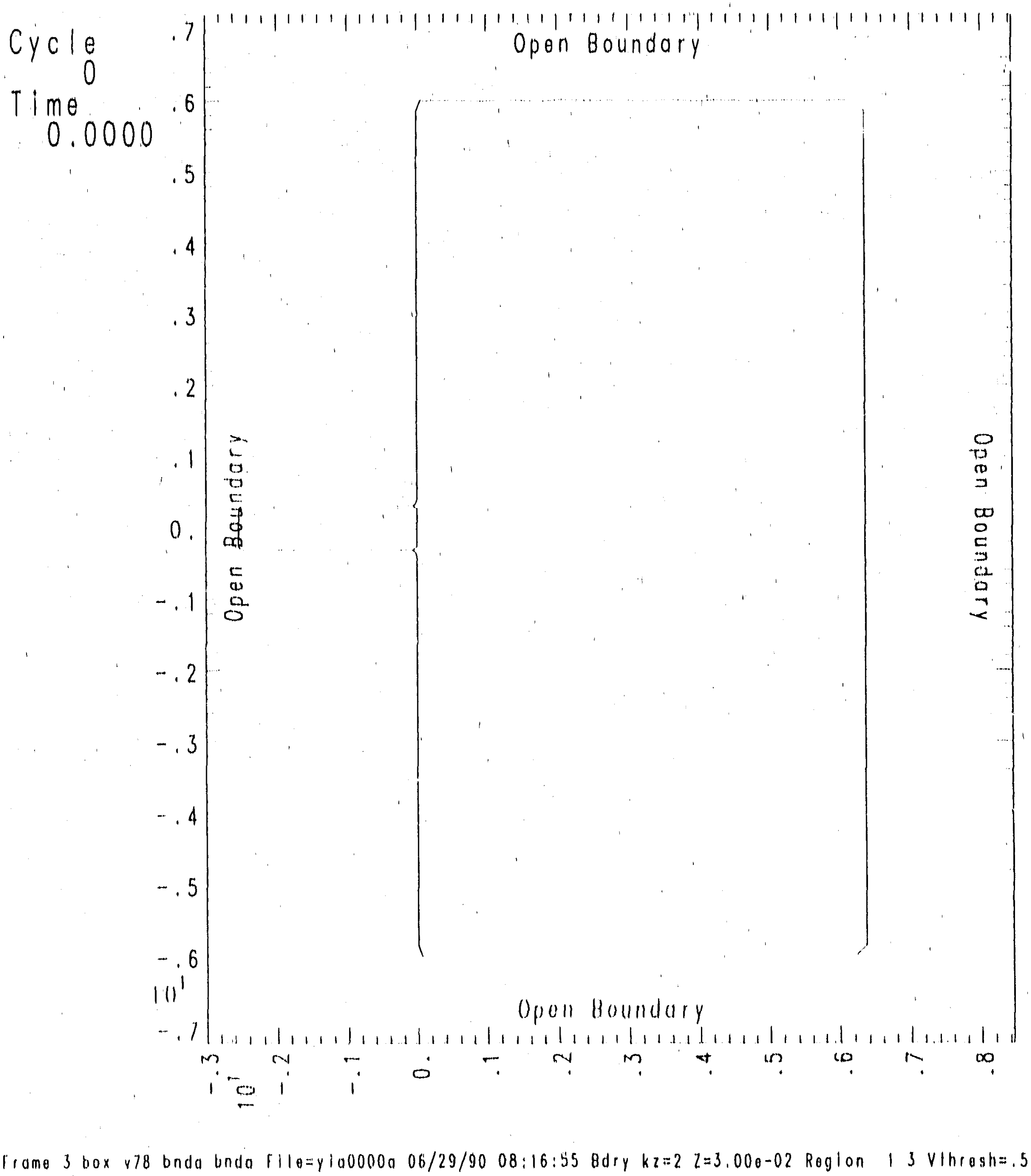

Figure A1. Yaw angle = 0°, time = 0.

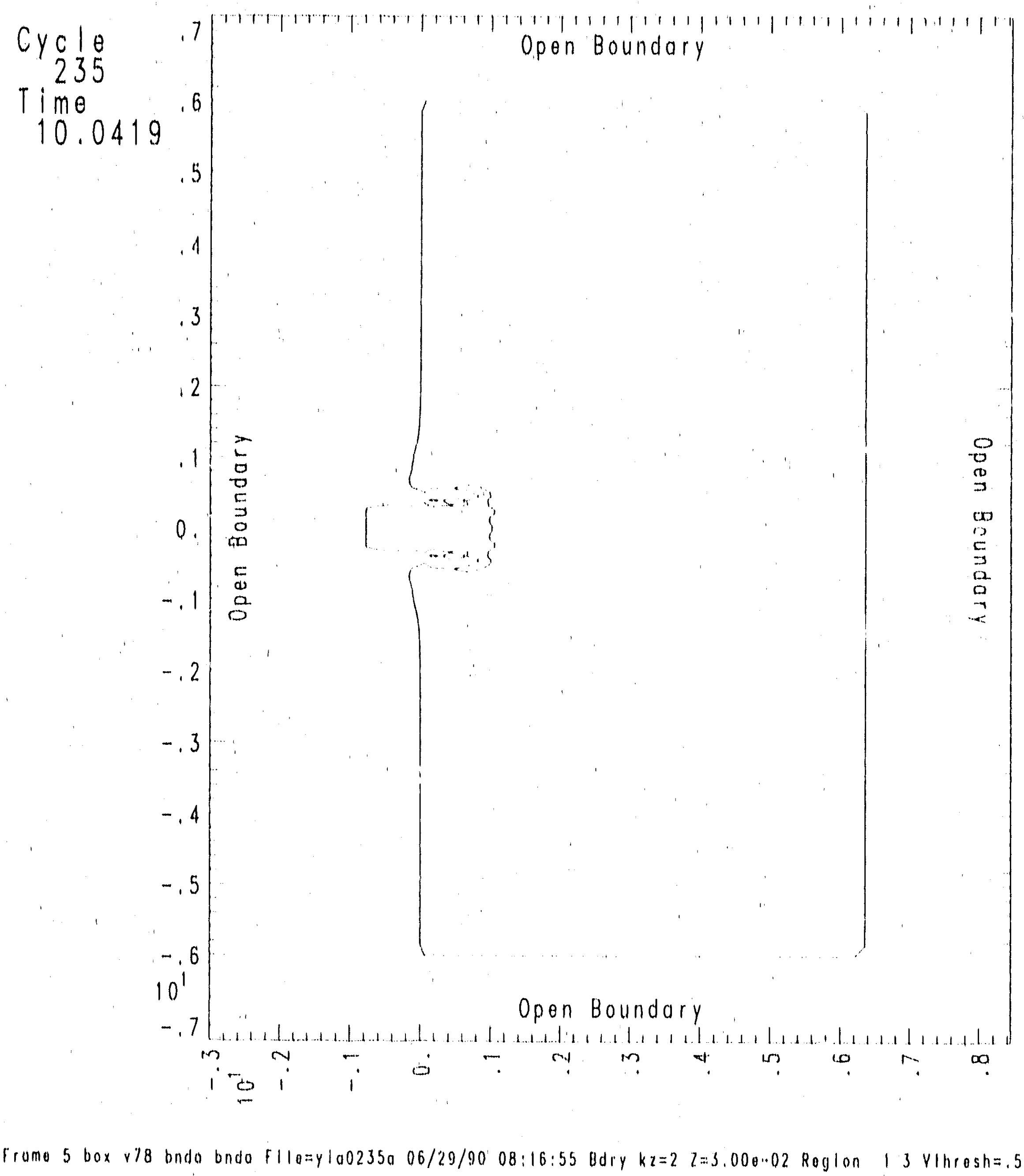

Figure A2. Yaw angle = 0°, time = 10 μs.

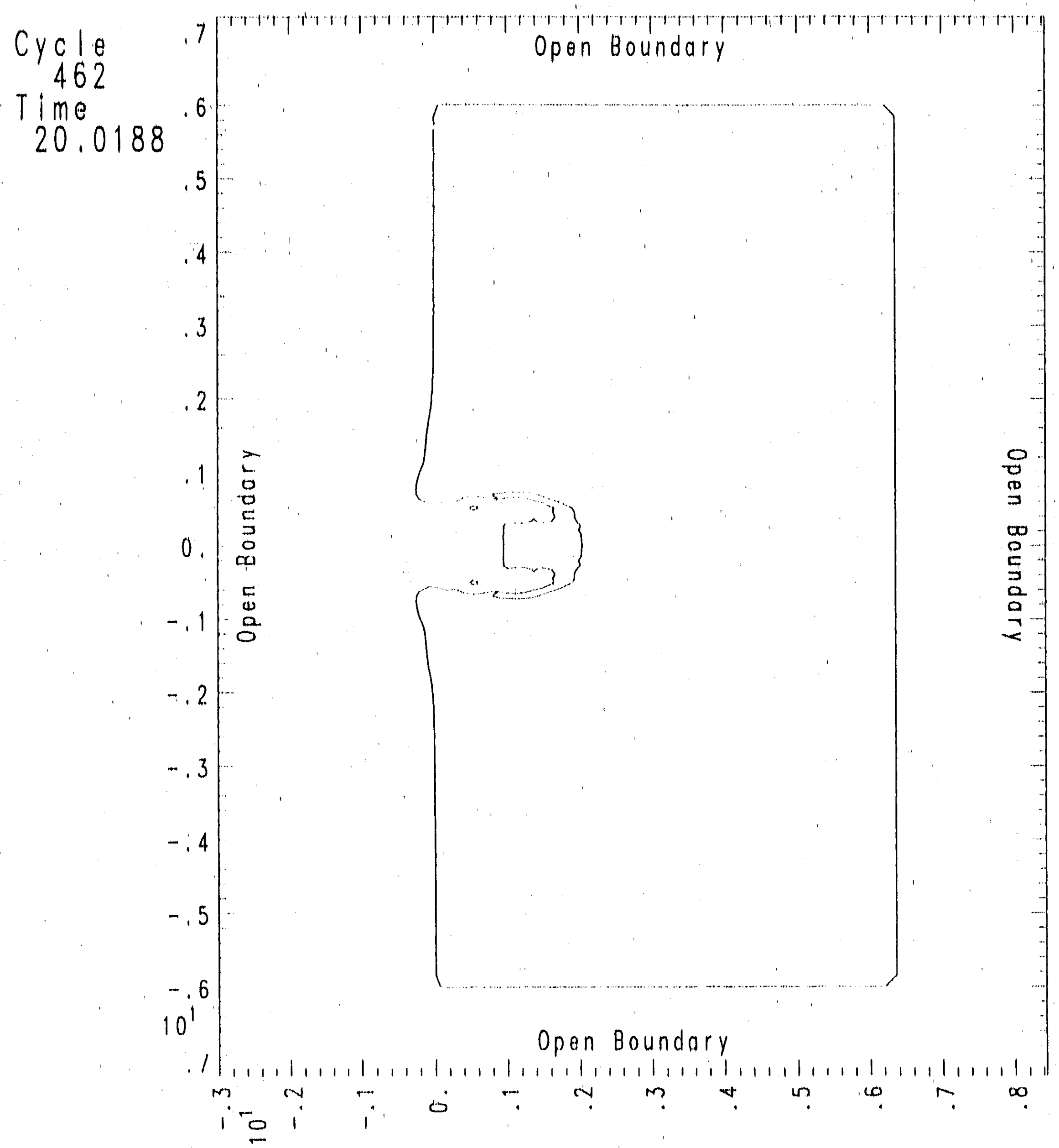

Figure A3. Yaw angle = 0°, time = 20 µs.

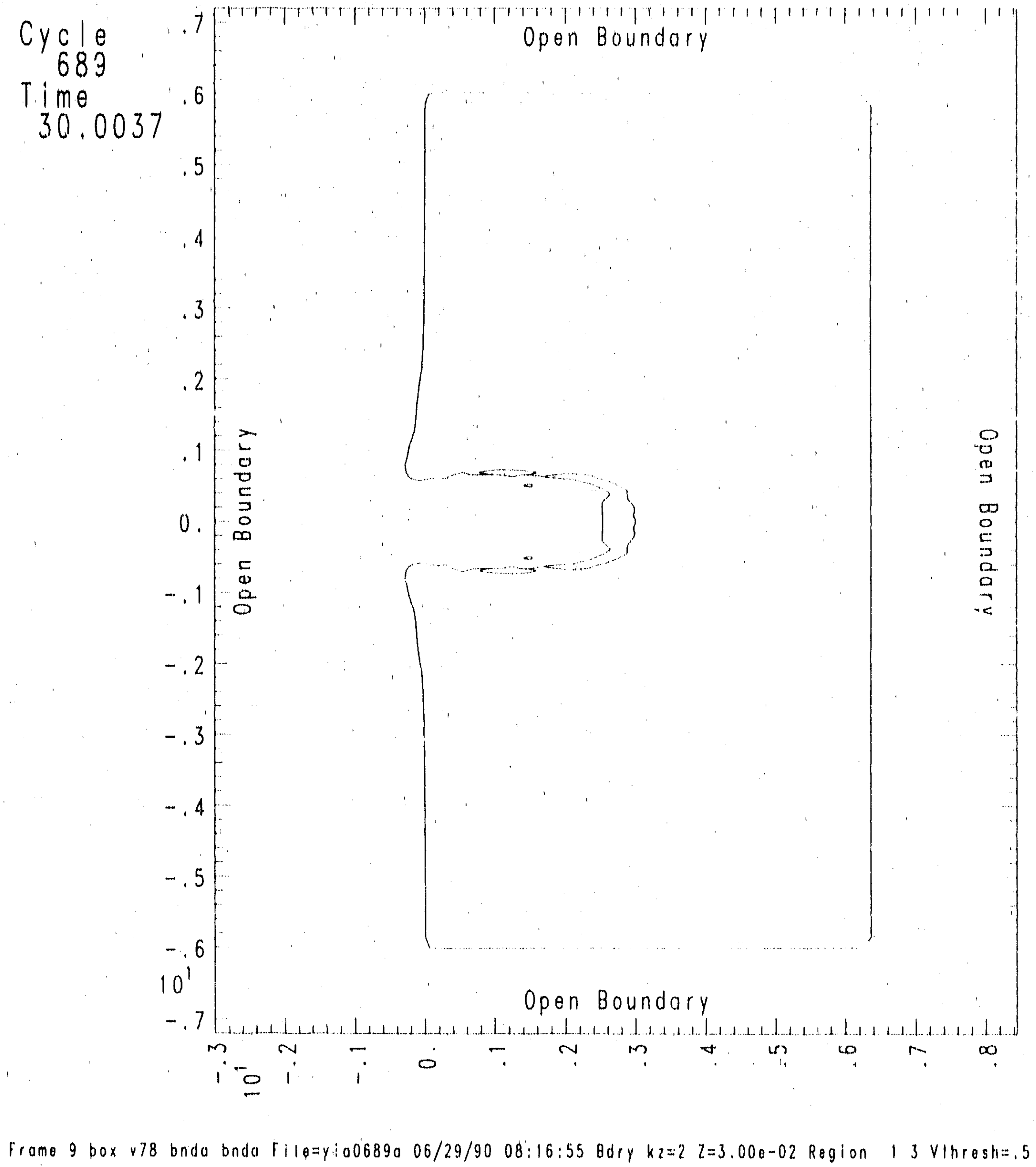

Figure A4. Yaw angle = 0°, time = 30 μs.

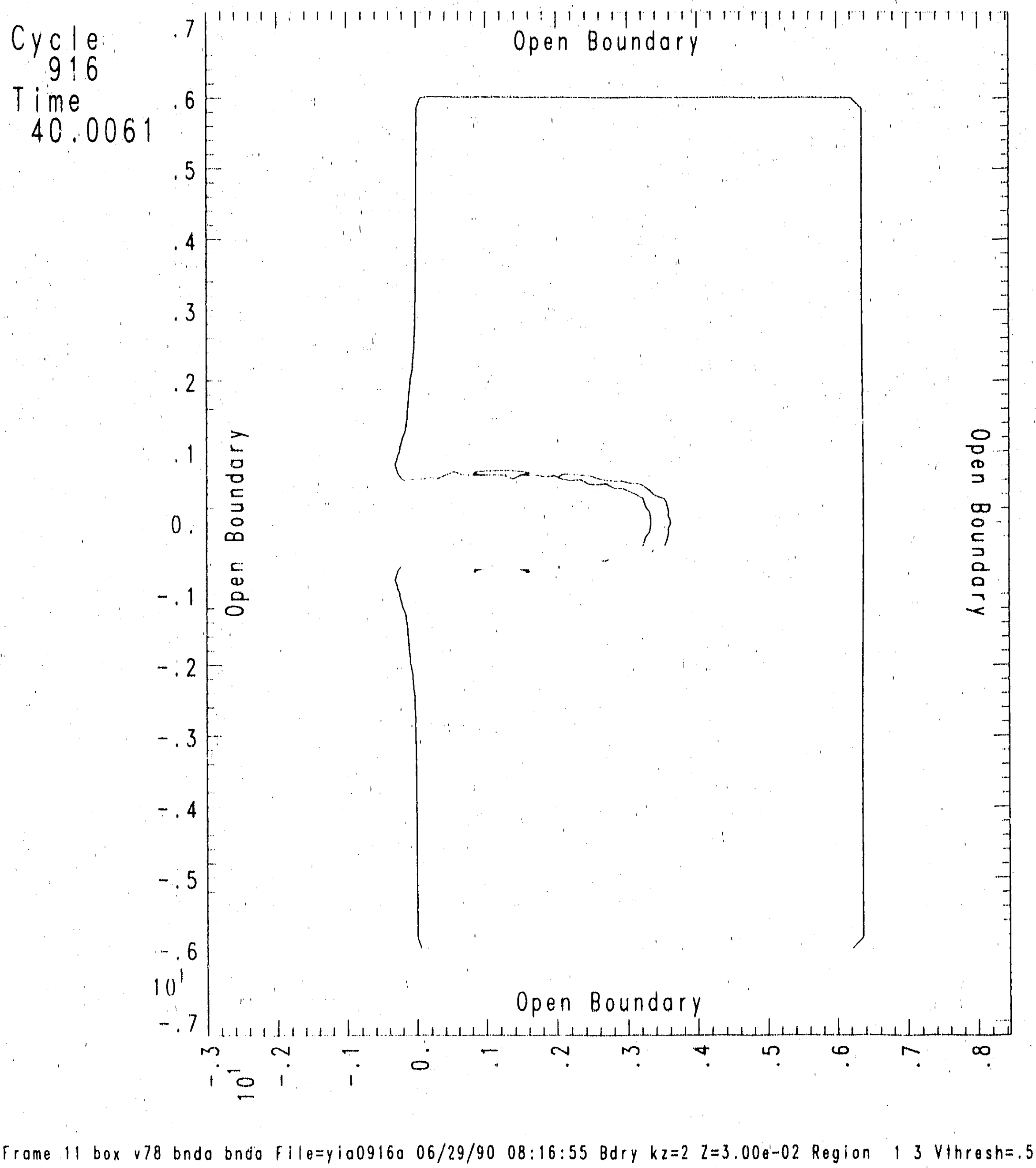

Figure A5. Yaw angle = 0°, time = 40 μs.

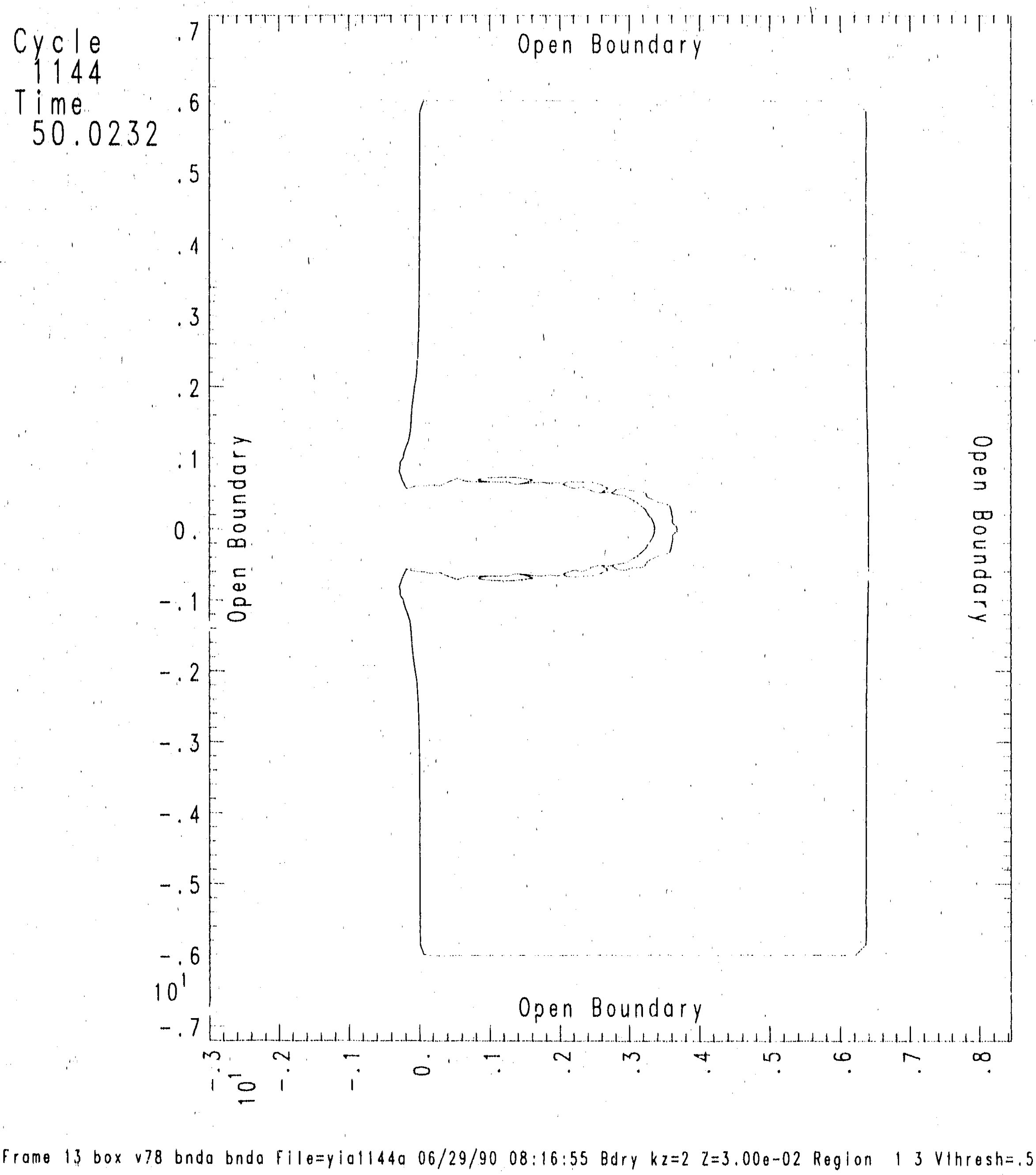

Figure A6. Yaw angle = 0°, time = 50 μs.

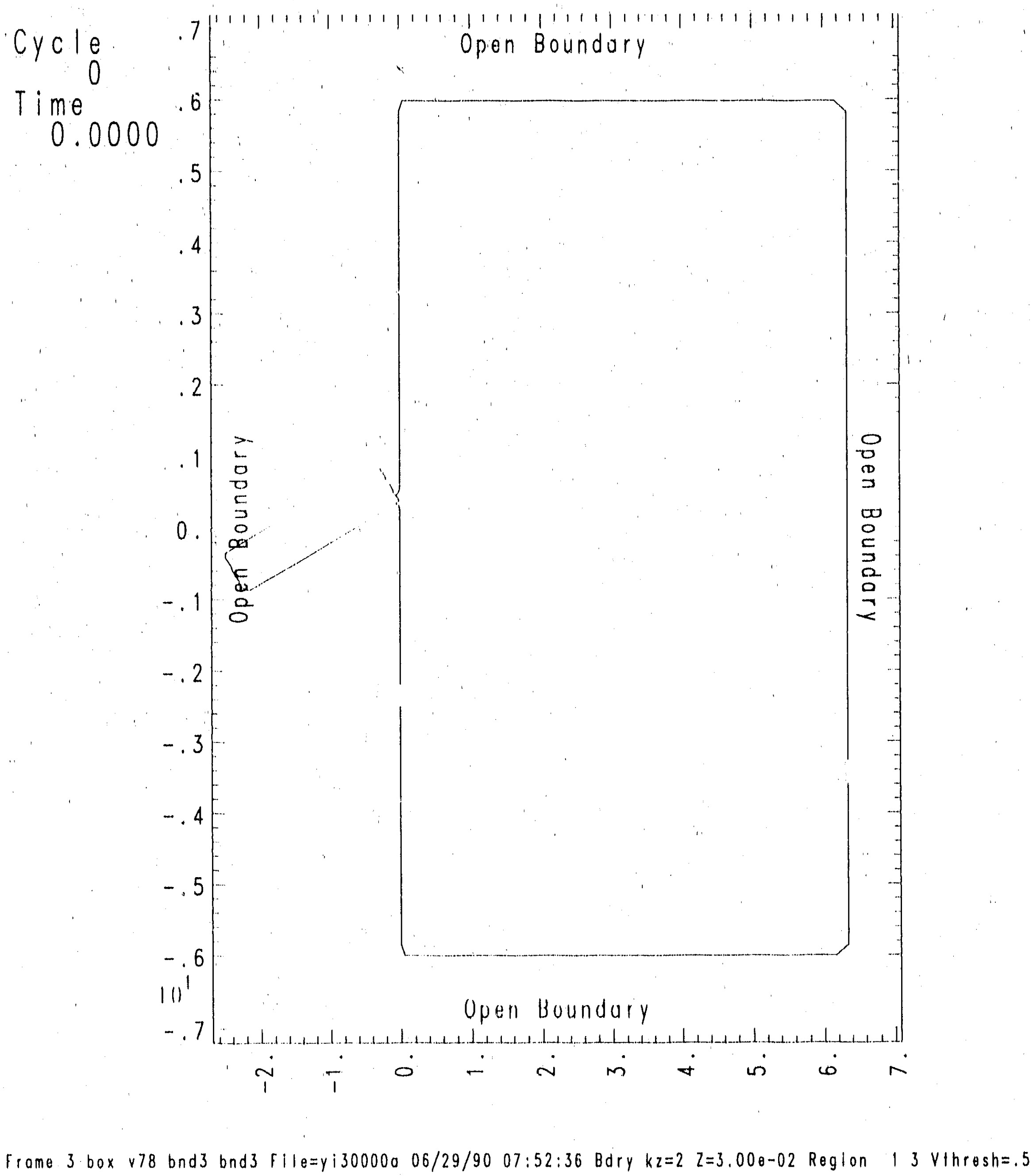

Figure A7. Yaw angle = 30°, time = 0.

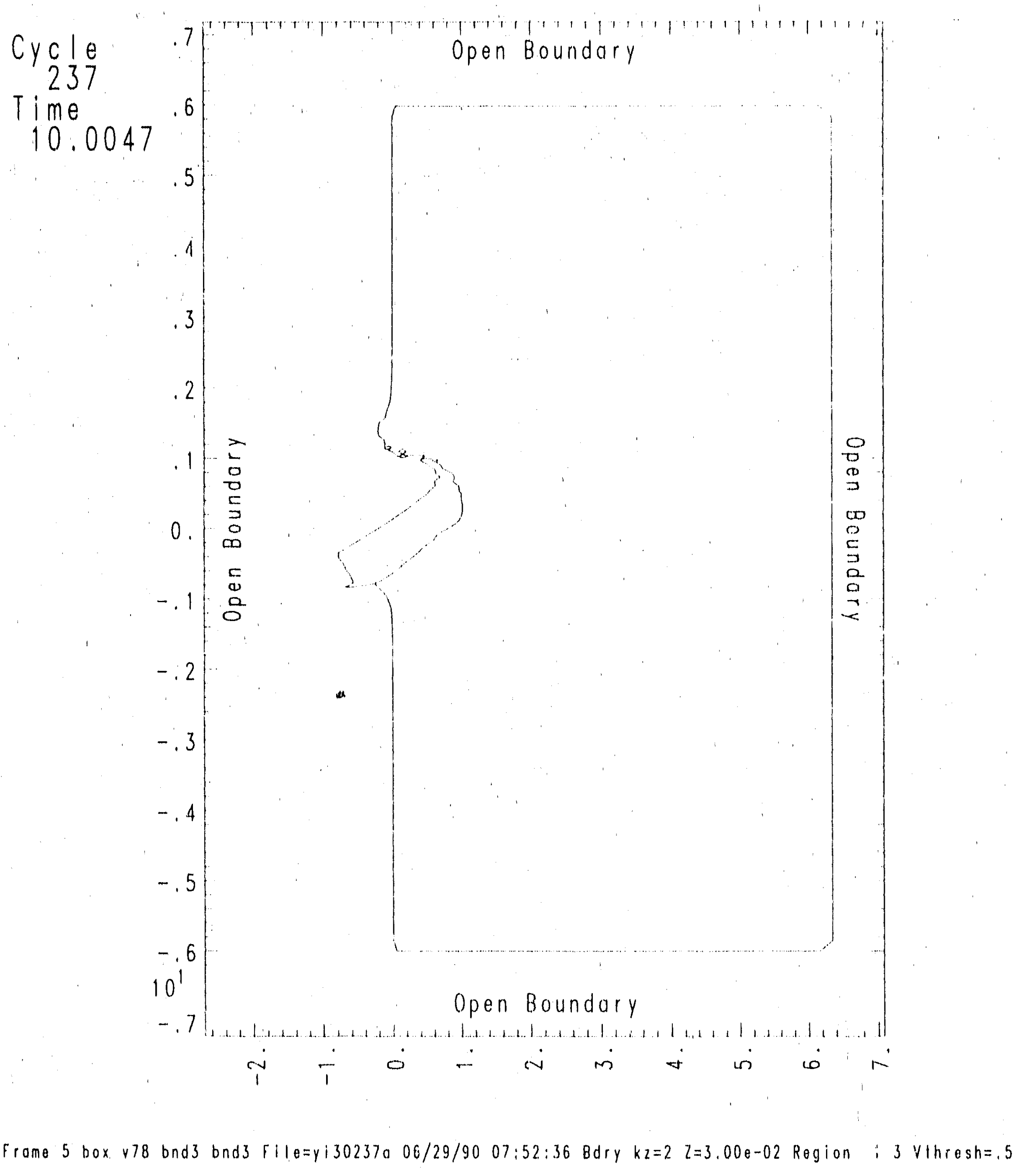

Figure A8. Yaw angle = 30°, time = 10 μs.

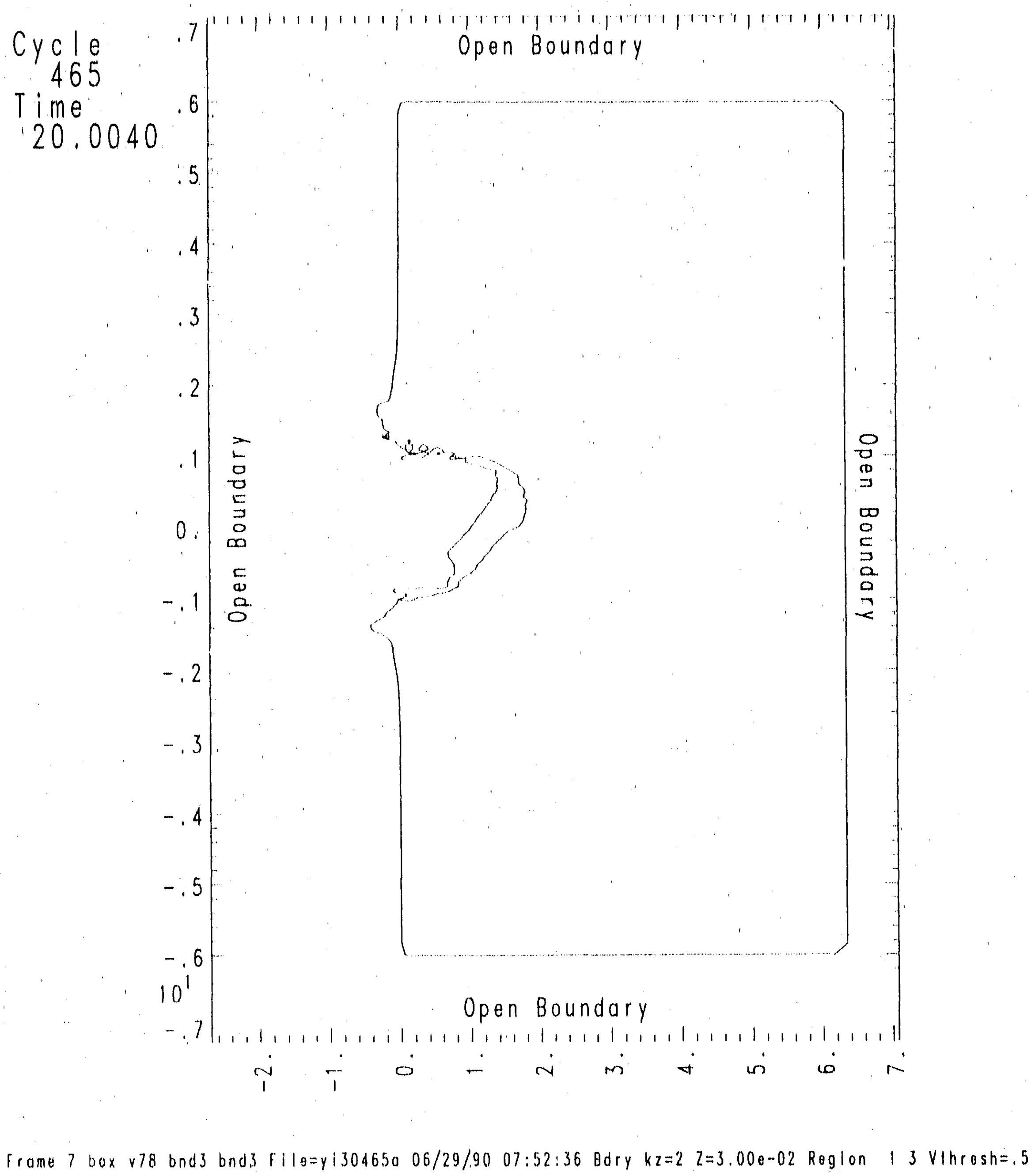

Figure A9. Yaw angle = 30°, time = 20 μs.

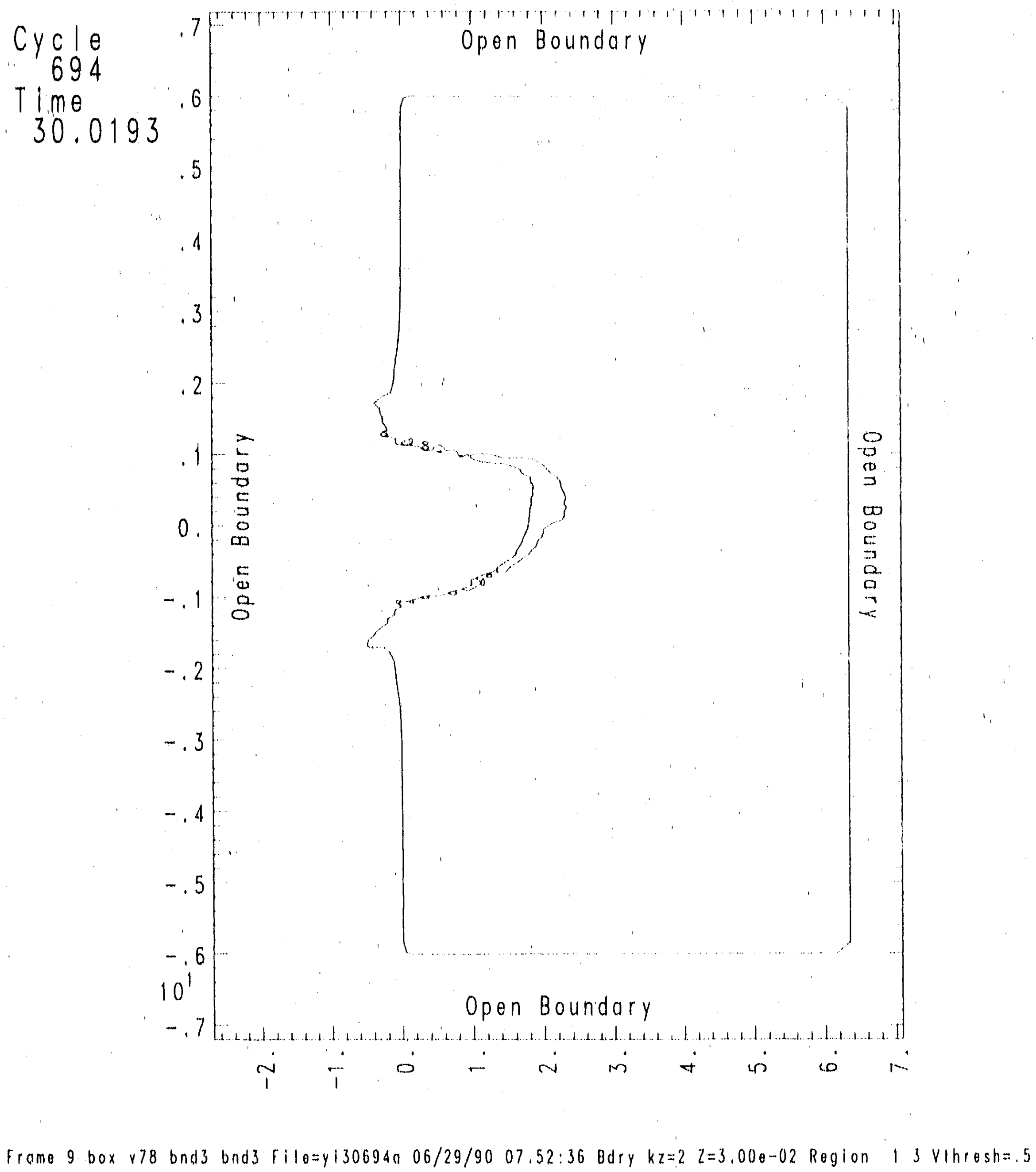

Figure A10. Yaw angle = 30°, time = 30 μs.

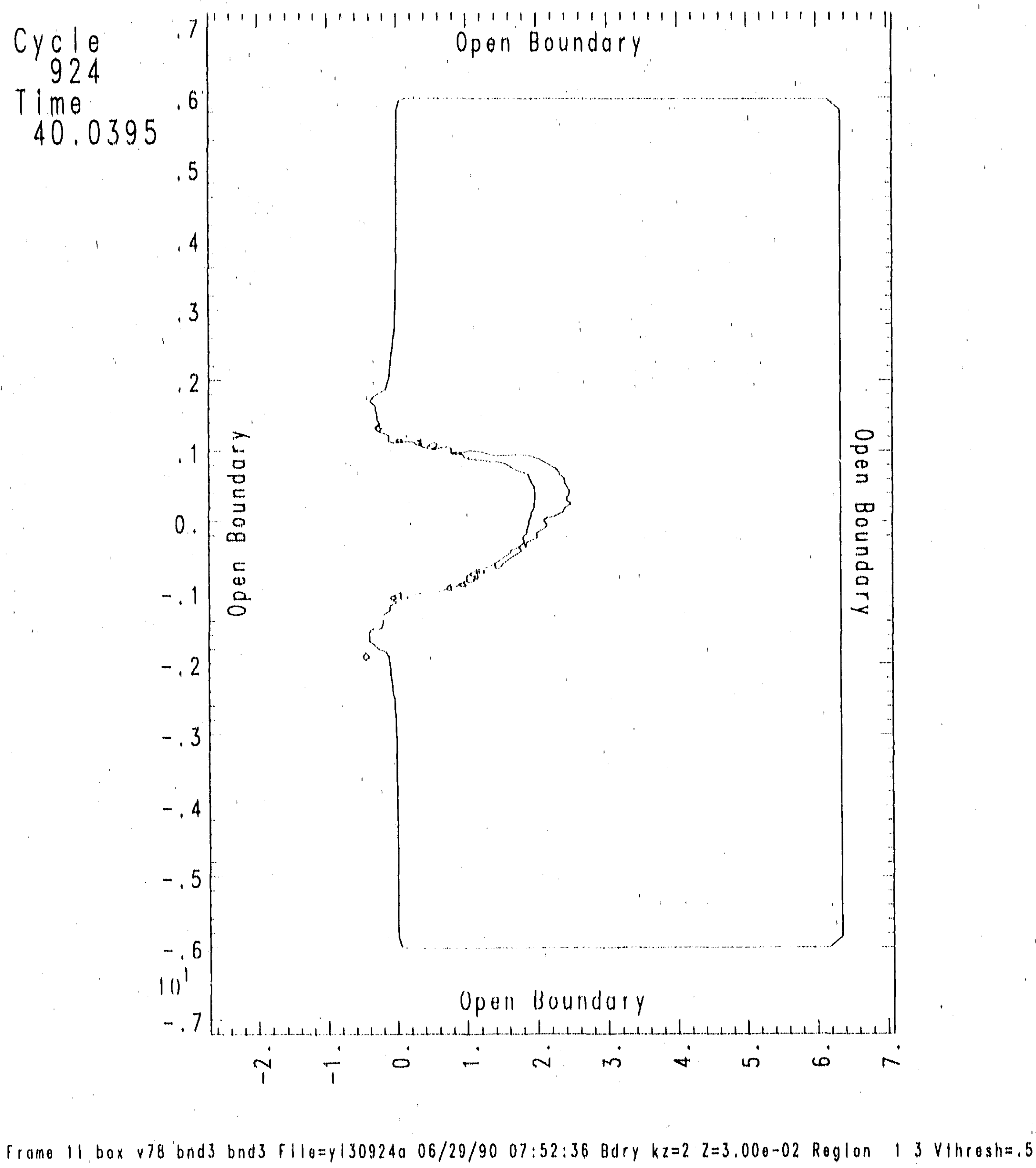

Figure A11. Yaw angle = 30°, time = 40 μs.

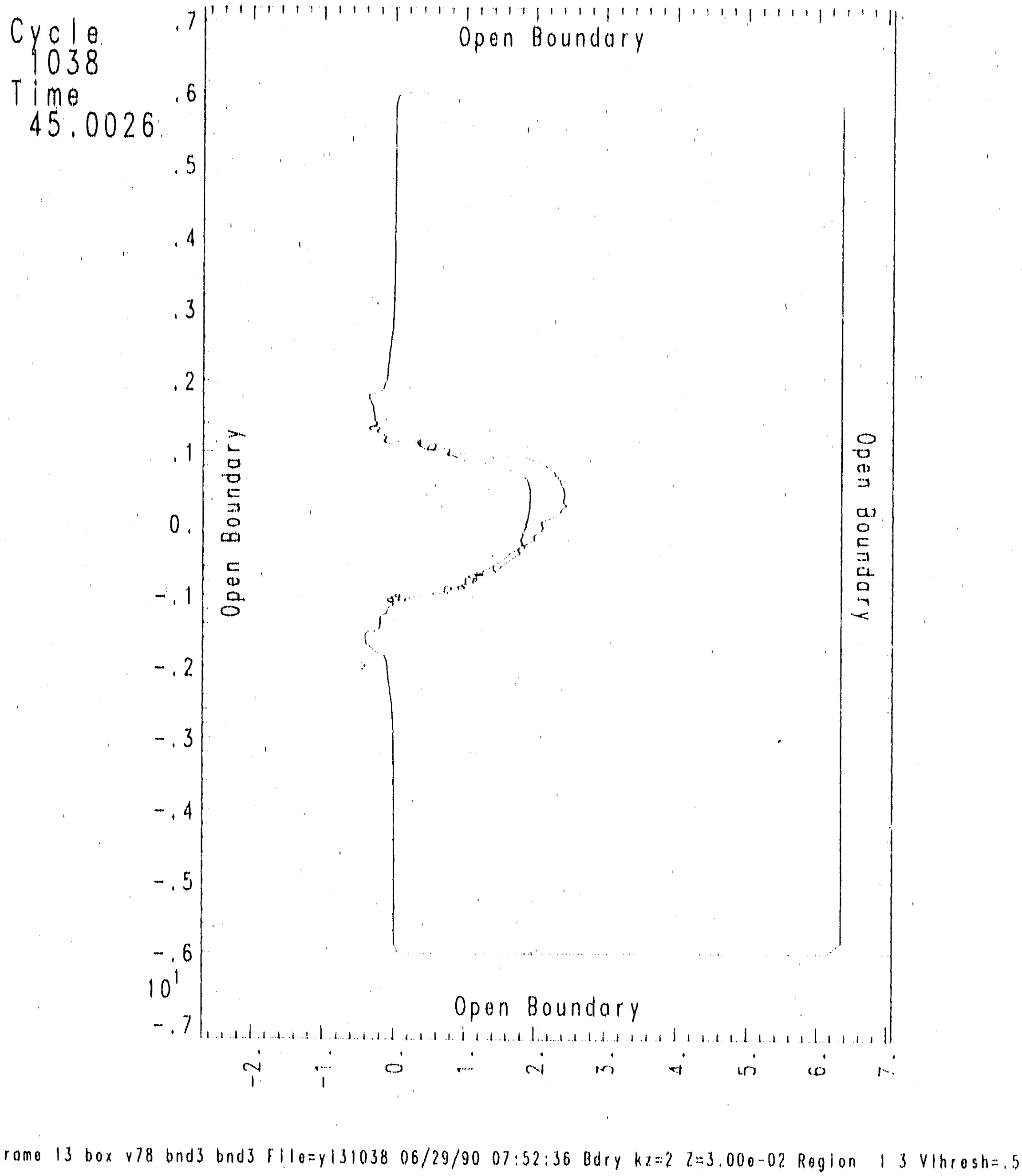

Figure A12. Yaw angle = 30°, time = 45 μs.

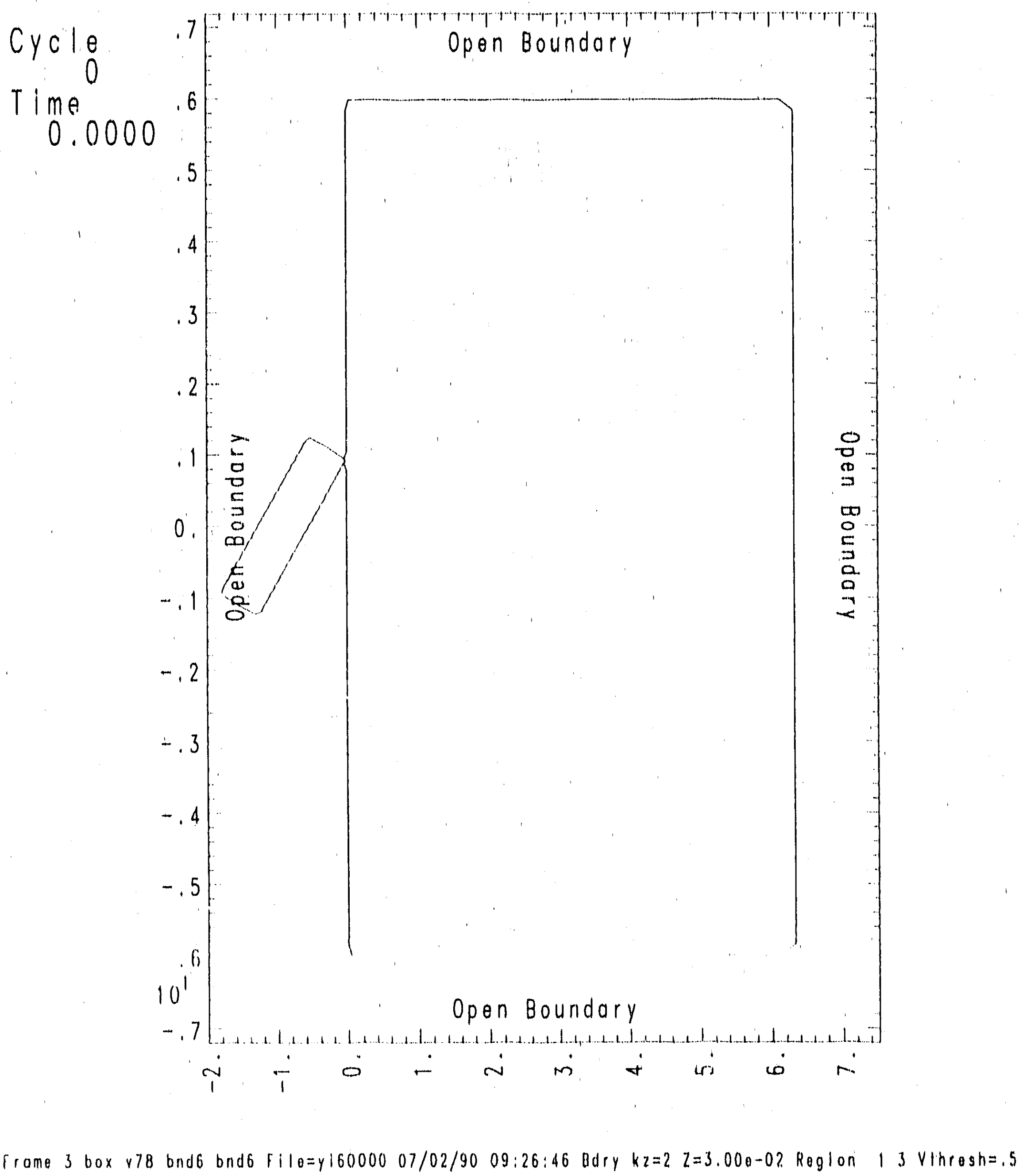

Figure A13. Yaw angle = 60°, time = 0.

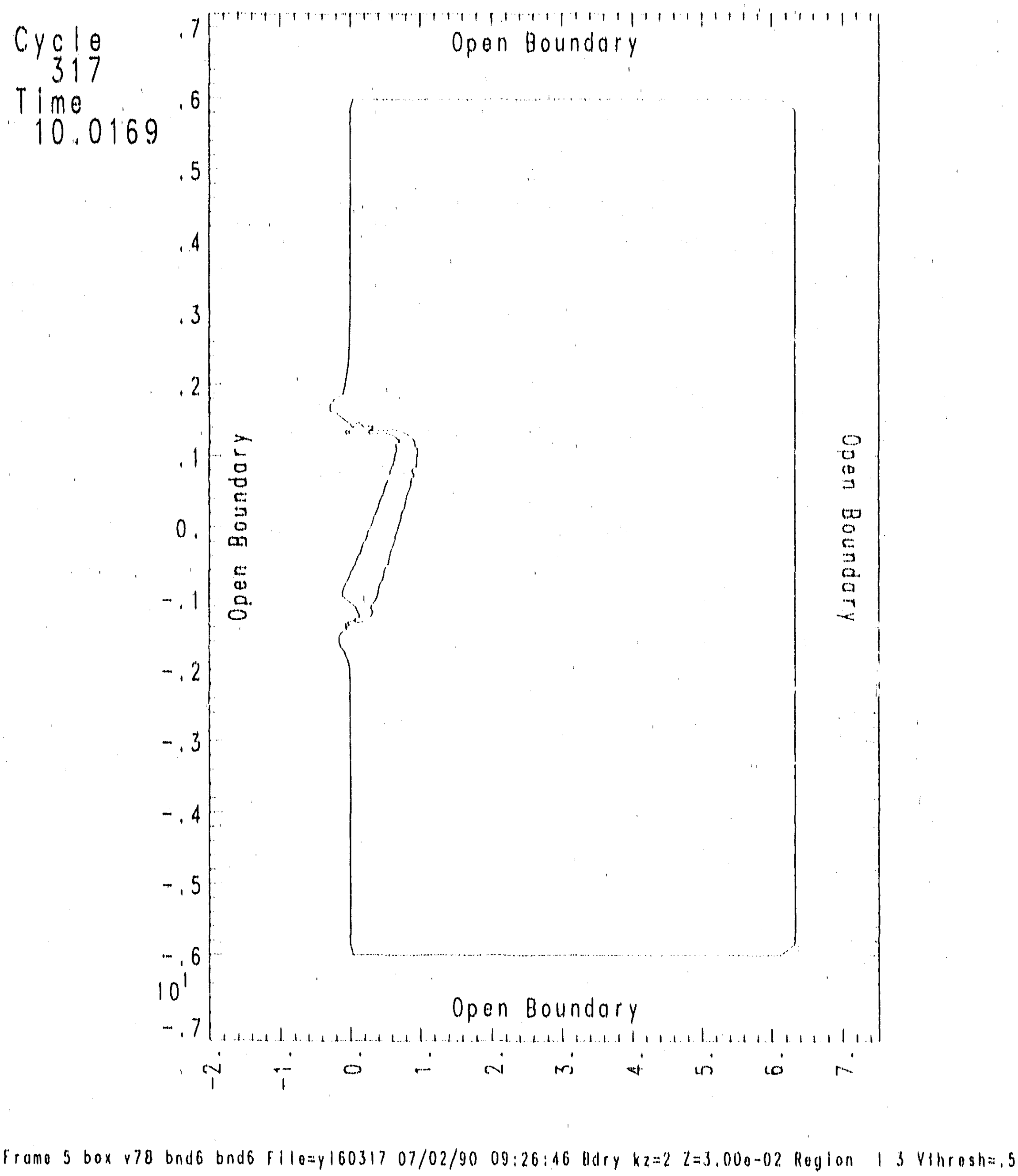

Figure A14. Yaw angle = 60°, time = 10 μs.

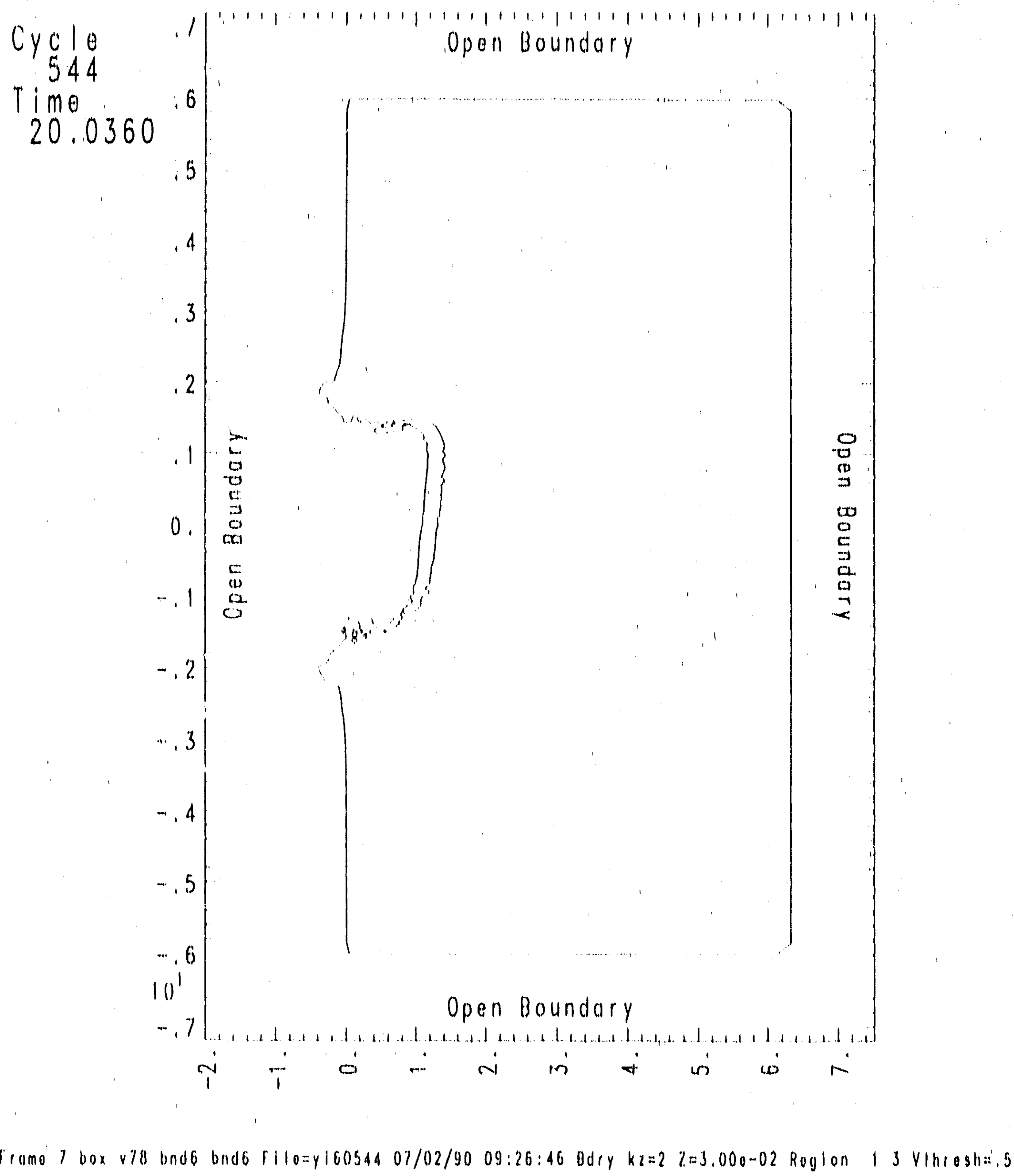

Figure A15. Yaw angle = 60°, time = 20 μs.

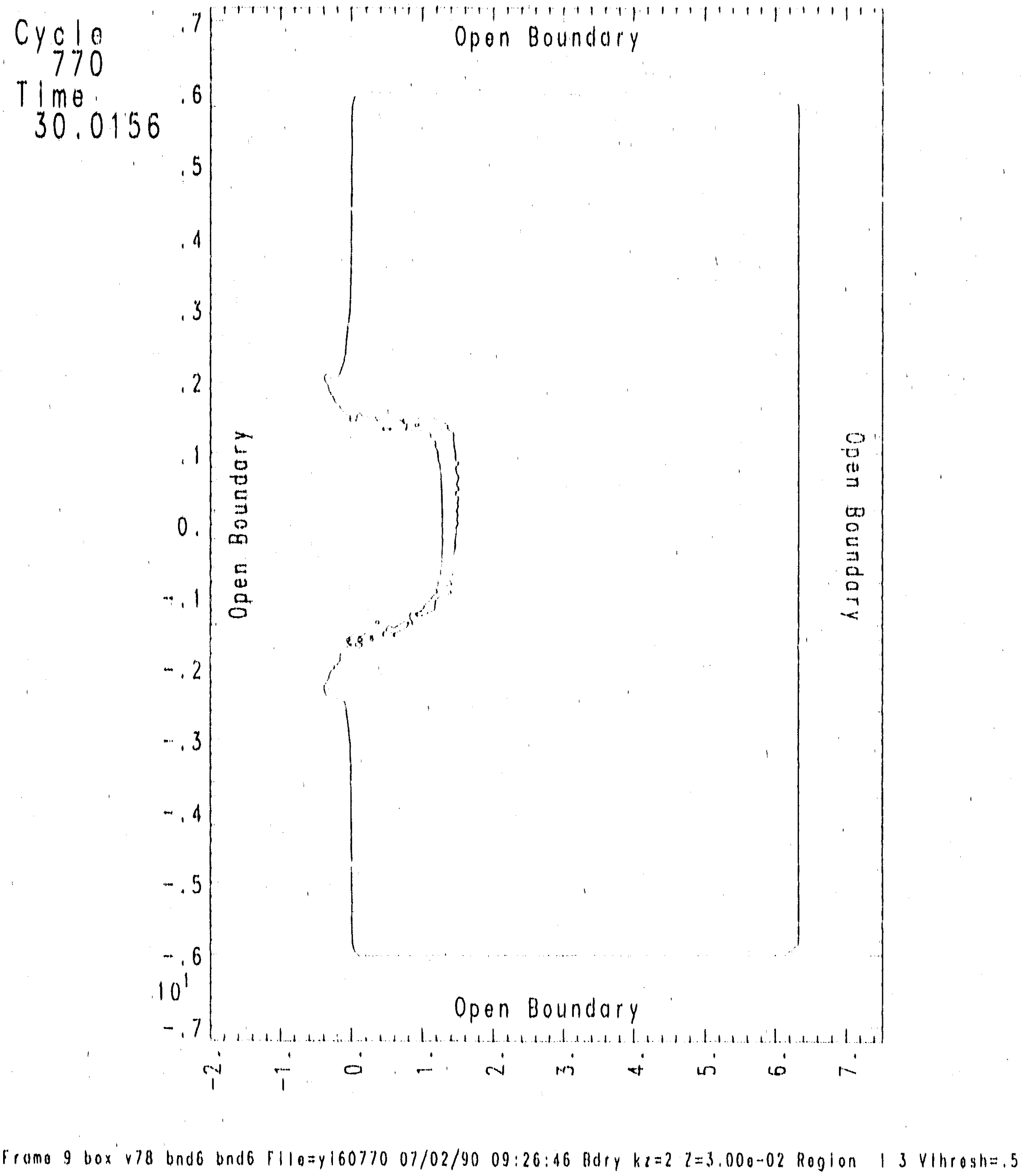

Figure A16. Yaw angle = 60°, time = 30 μs.

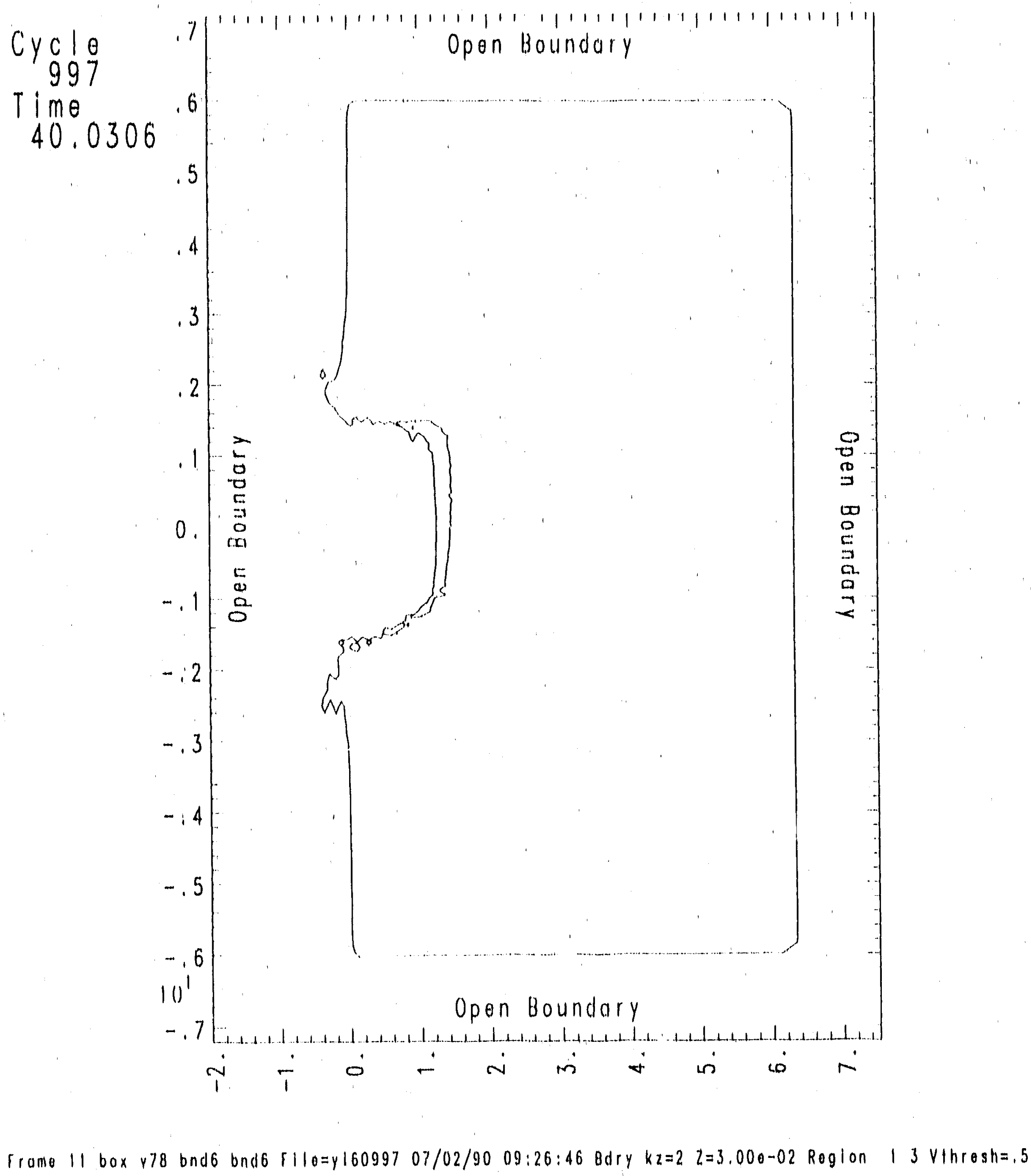

Figure A17. Yaw angle = 60°, time = 40 μs.

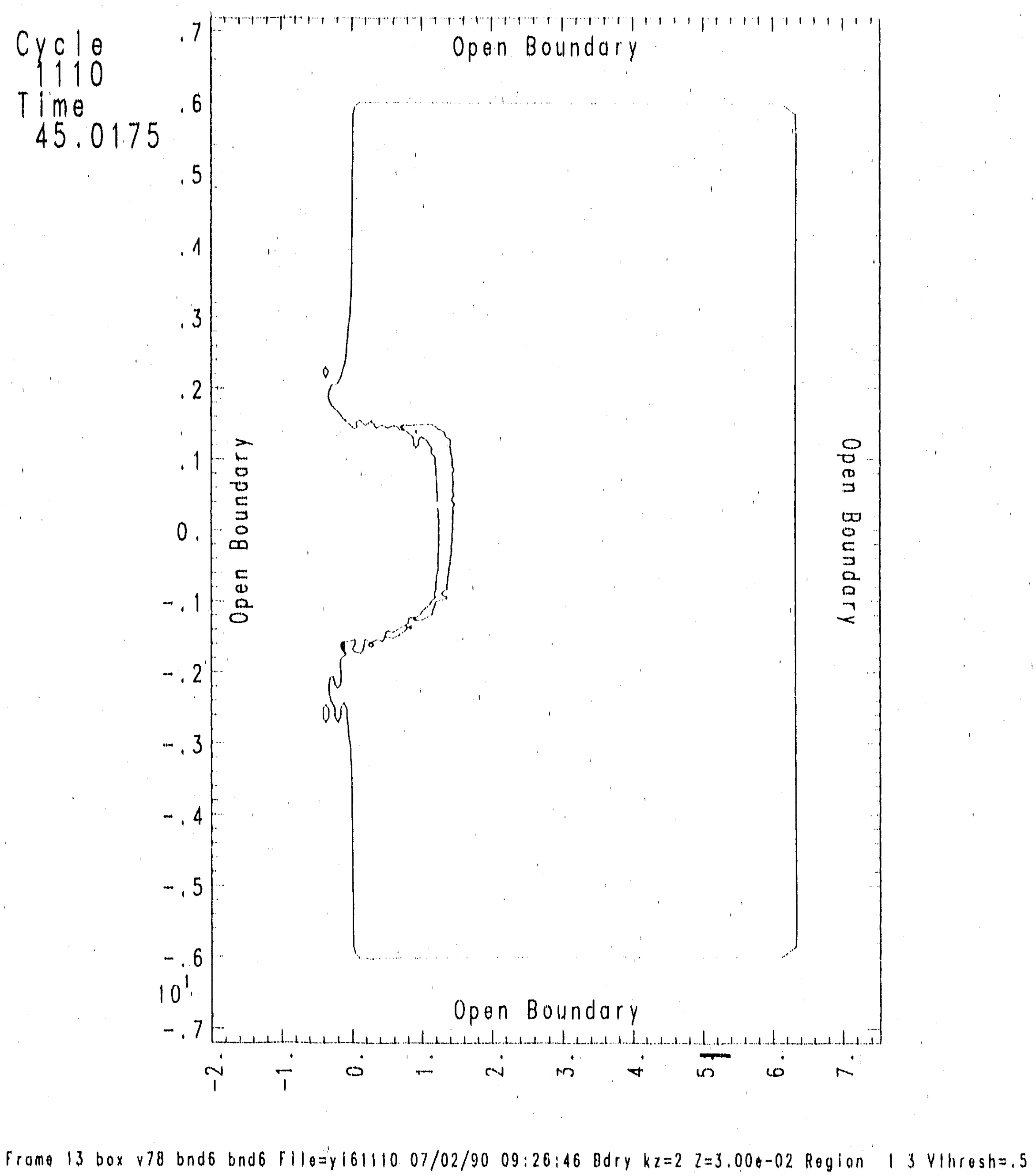

Figure A18. Yaw angle = 60°, time = 45 μs.

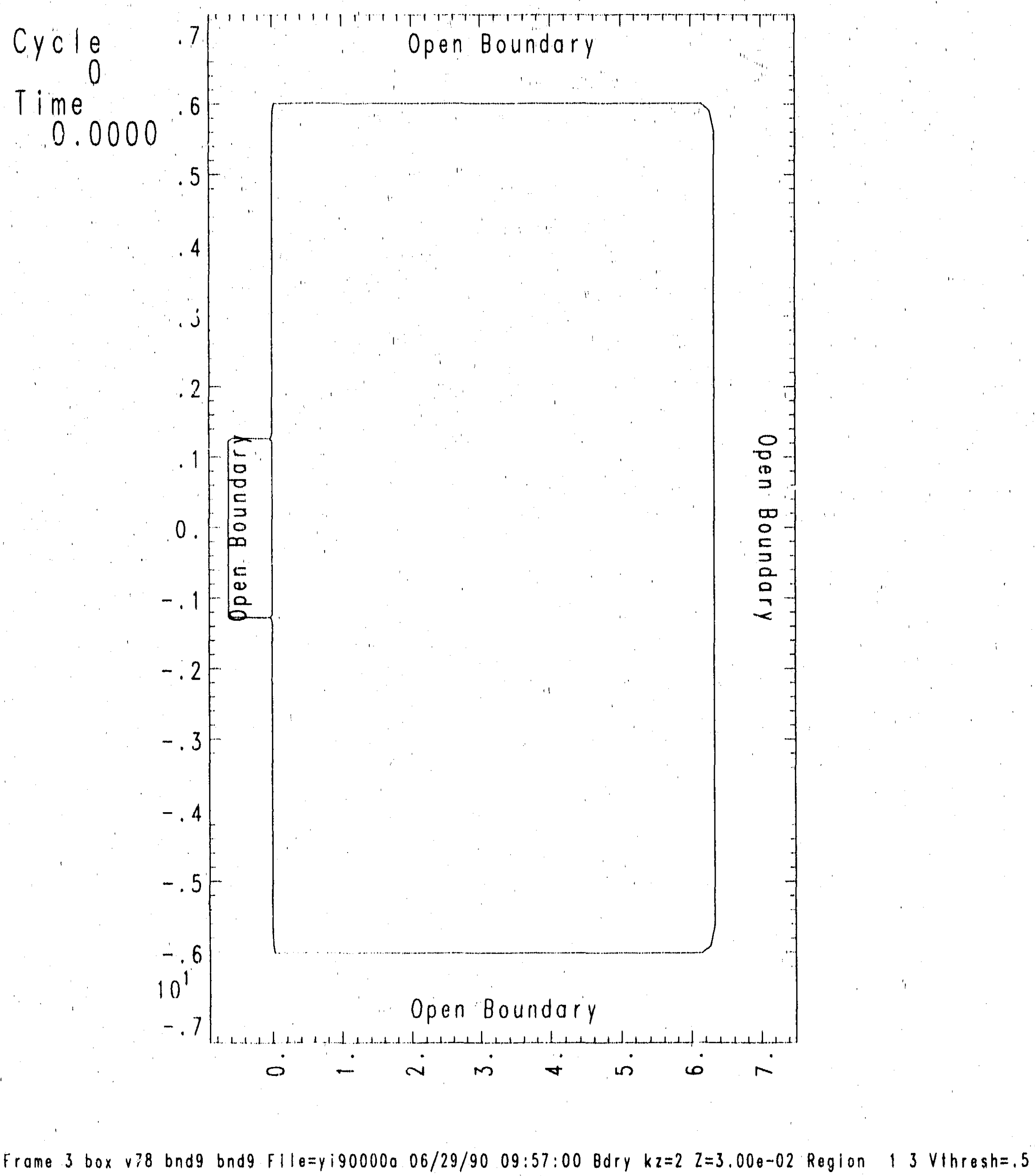

Figure A19. Yaw angle = 90°, time = 0.

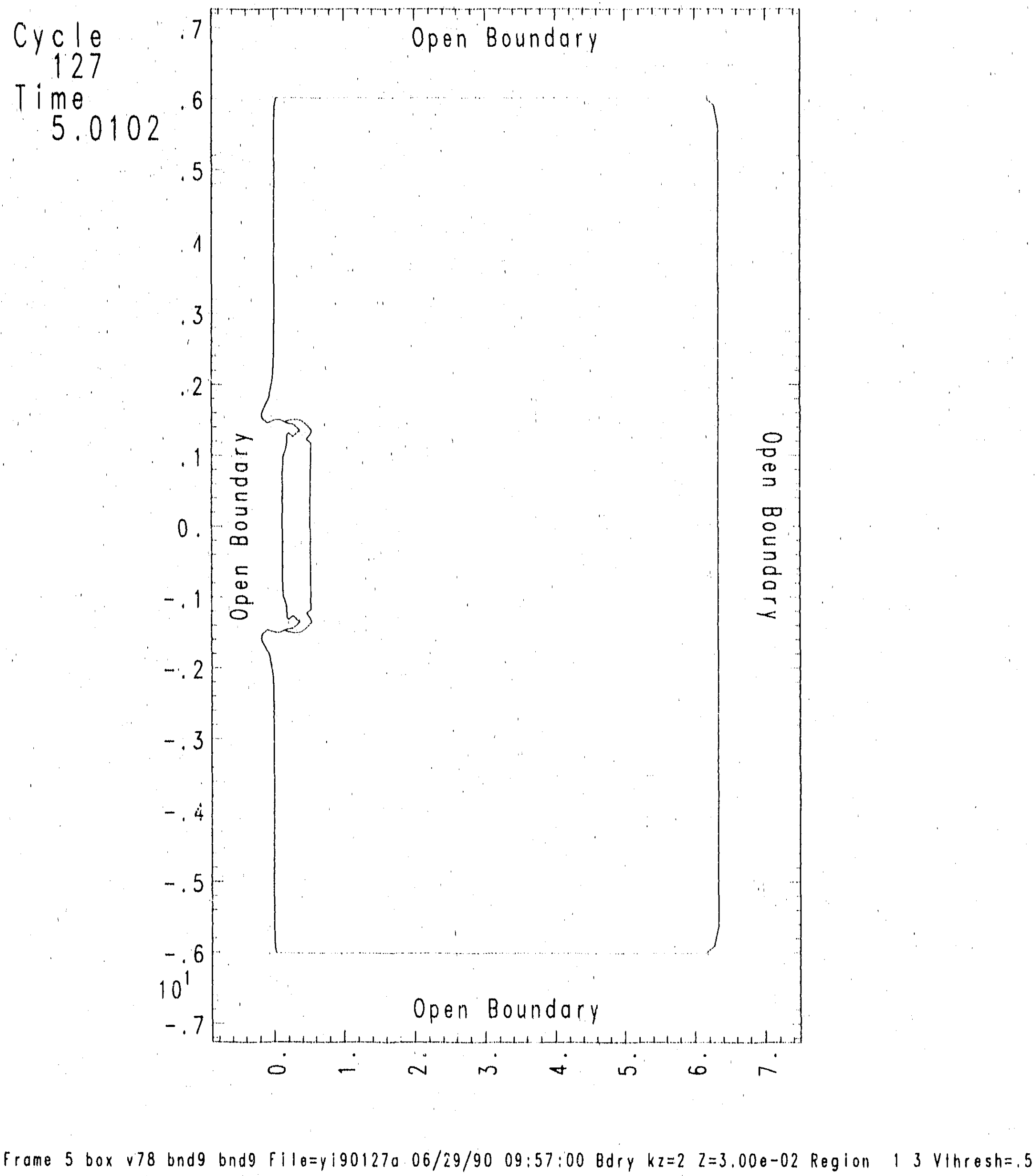

Figure A20. Yaw angle = 90°, time = 5 μs.

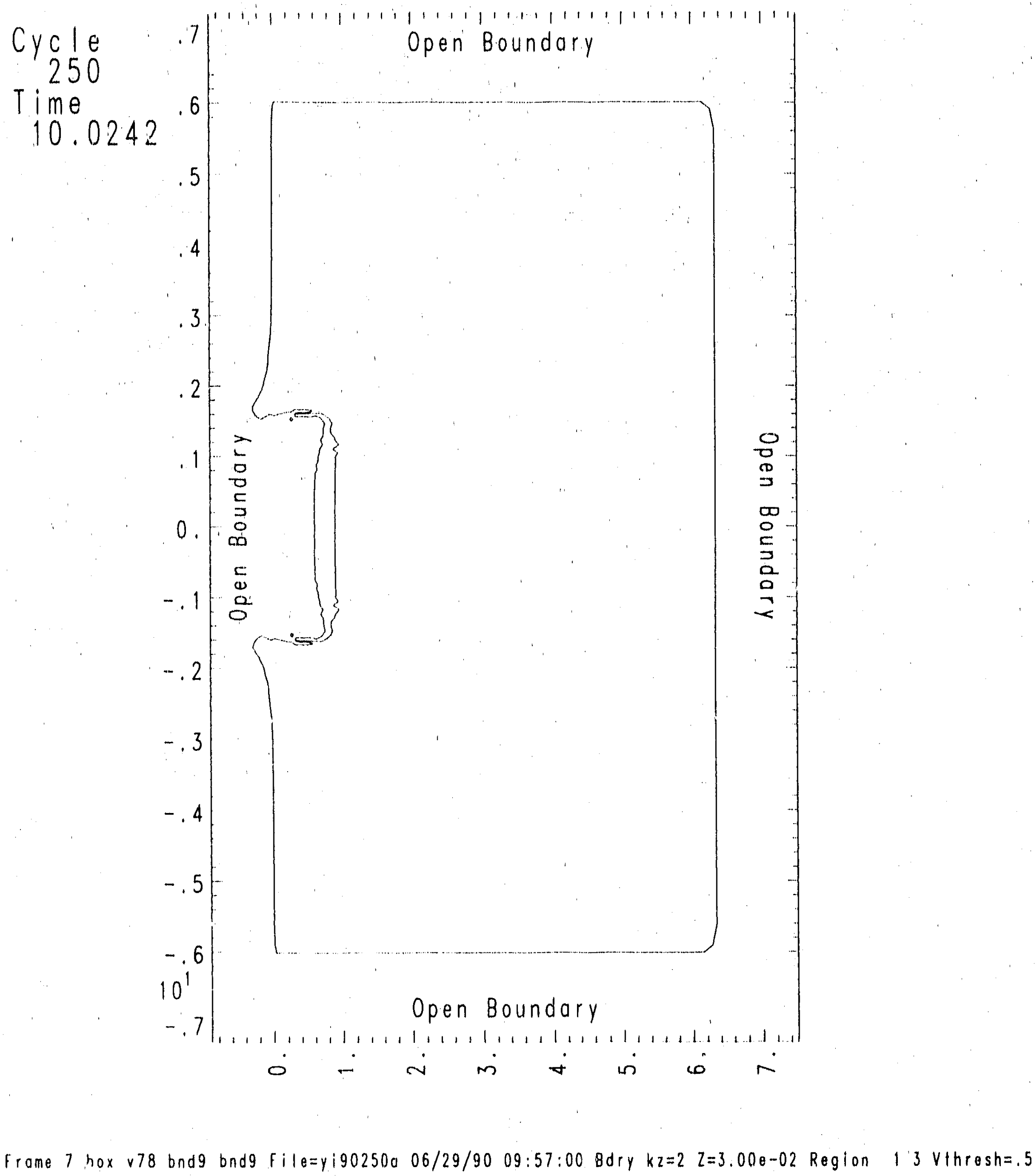

Figure A21. Yaw angle = 90°, time = 10 µs.

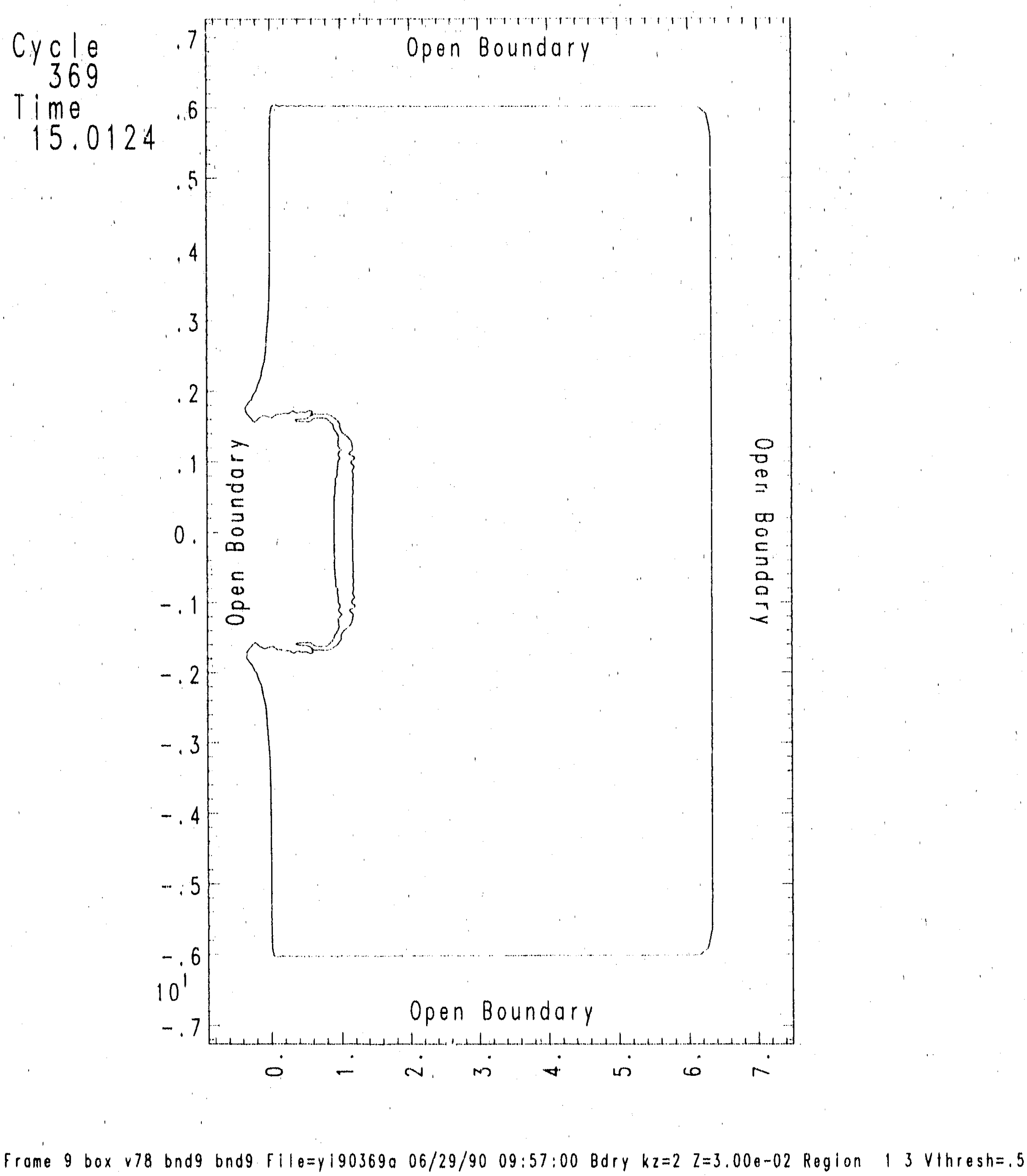

Figure A22. Yaw angle = 90°, time = 15 μs.

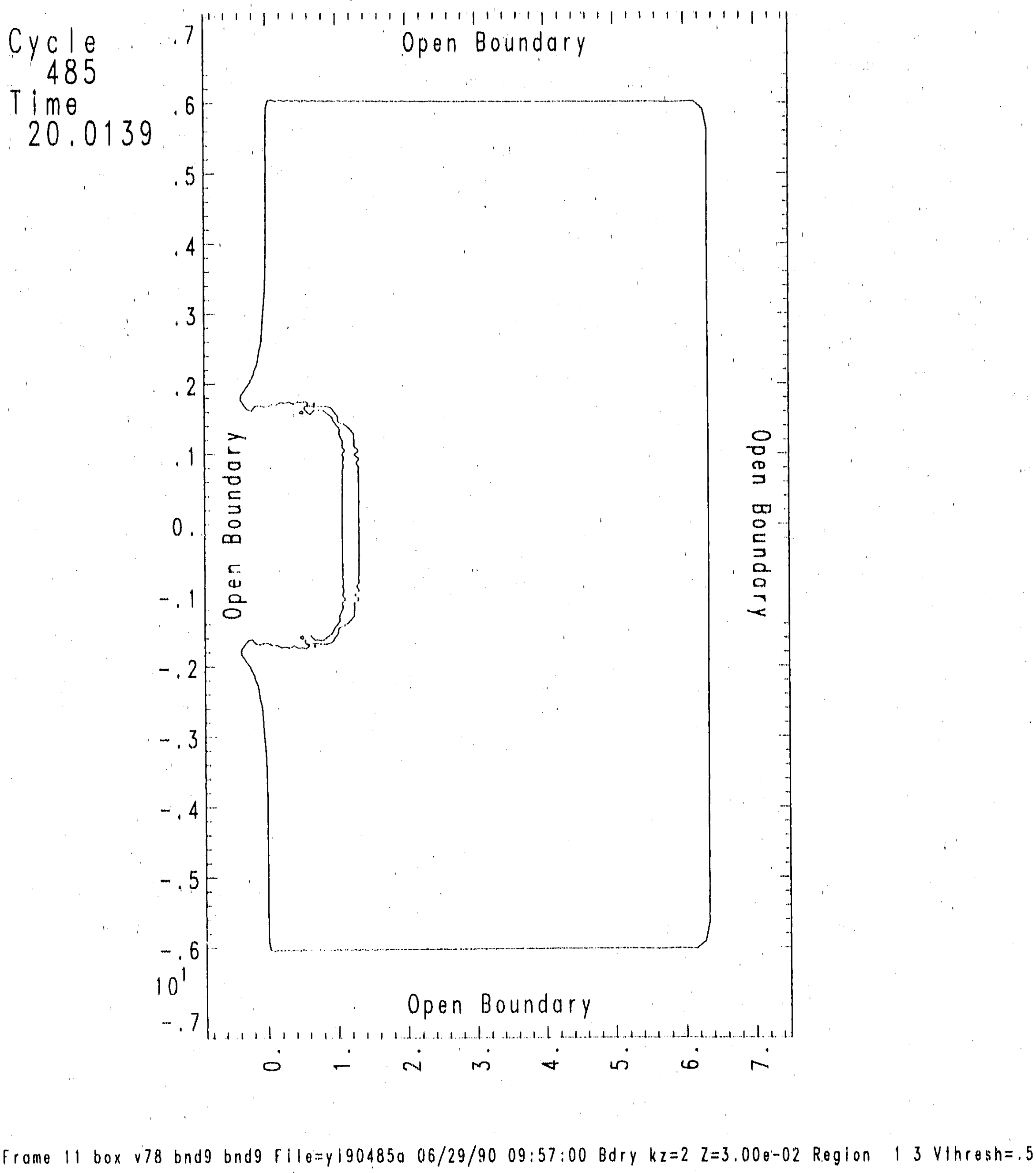

Figure A23. Yaw angle = 90°, time = 20 μs.

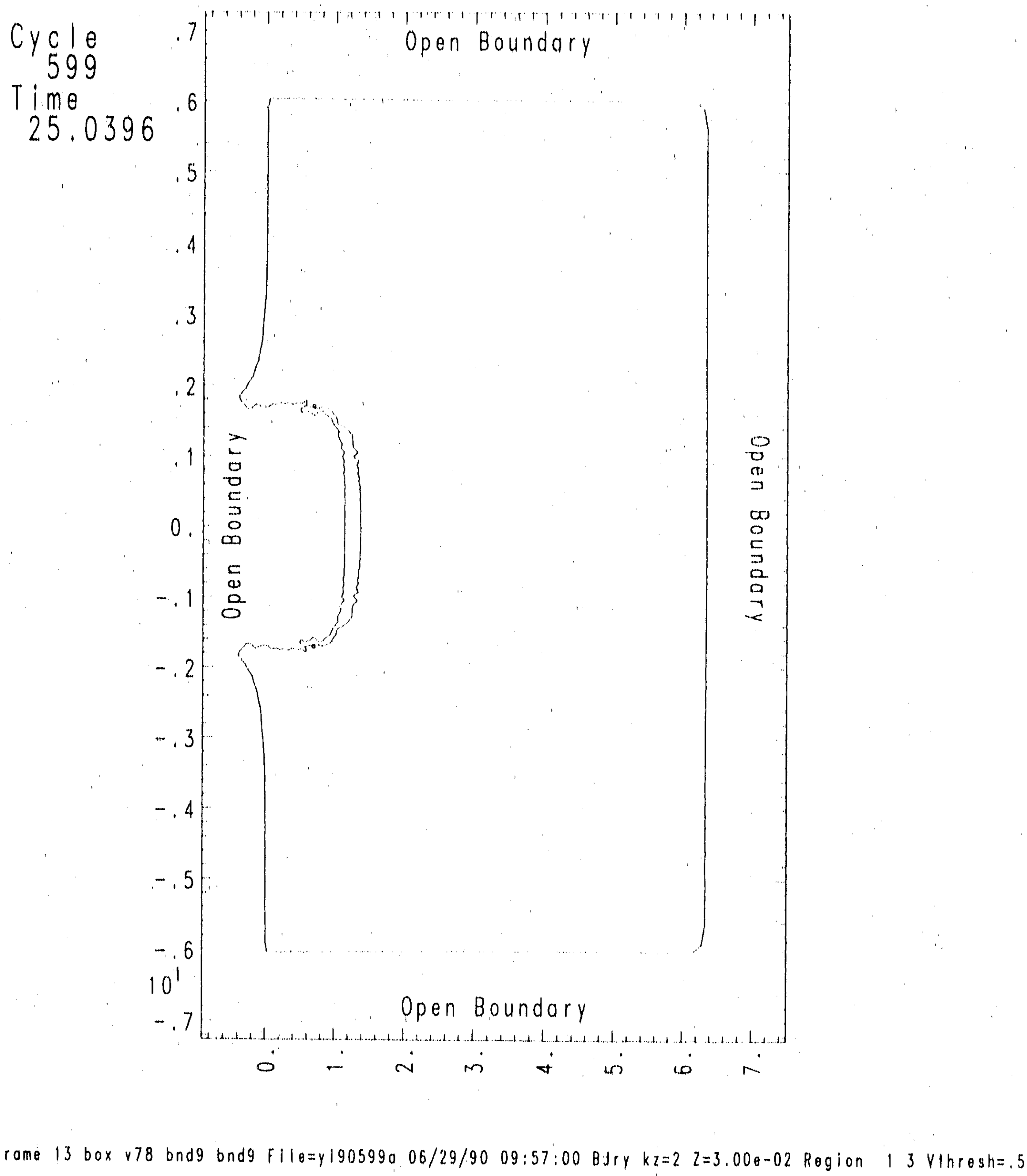

Figure A24. Yaw angle = 90°, time = 25 μs.

END

DATE FILMED

11 / 27 / 90